
Antennas for detection of ADS-B signals at satellites and investigation on crosstalk between antenna elements

For detection of ADS-B signals

Master thesis
Karsten Schou Nielsen

Aalborg University
Department of Electronic Systems
Fredrik Bajers Vej 7B
DK-9220 Aalborg



AALBORG UNIVERSITY

STUDENT REPORT

Department of Electronic Systems

Fredrik Bajers Vej 7
DK-9220 Aalborg Ø
<http://es.aau.dk>

Title:

Antennas for Cube Satellites in Low Earth Orbit for detection of ADS-B

Theme:**Project Period:**

2019

Project Group:**Abstract:**

This project investigates different antenna types for mounting on a cube satellite for reception of ADS-B. The report is split up in two parts, where the first part is a link-budget that sets the requirements for the antenna. The second part is where the antennas are investigated. This includes a reflector antenna, a quadrifilar antenna and a hemispherical antenna.

Participant(s):

Karsten Schou Nielsen

Supervisor(s):

Ming Shen

Copies: 0**Page Numbers:** 51**Date of Completion:**

May 6, 2019

The content of this report is freely available, but publication (with reference) may only be pursued due to agreement with the author.



AALBORG UNIVERSITET

STUDENTERRAPPORT

Institut for Elektroniske Systemer

Fredrik Bajers Vej 7

DK-9220 Aalborg Ø

<http://es.aau.dk>

Titel:

Antenna for Cube Satellites in Low Earth Orbit for detection of ADS-B

Tema:**Projektperiode:**

2019

Projektgruppe:**Deltager(e):**

Karsten Schou Nielsen

Vejleder(e):

Ming Shen

Oplagstal: 0**Sidetal:** 51**Afleveringsdato:**

6. maj 2019

Abstract:

I dette projekt er der blevet undersøgt hvilke antenner der kan bruges til at modtage ADS-B signaler på en cube satellit. Rapporten er delt op i to hvor den første del er opstillet som et linkbudget der beskriver kravende til en sådan antennen. Den anden del er selve undersøgesøgelsen af forskellige antennetyper. Disse inkluderer en parabol antennen, en quadrifilar helical antenna og en hemispherical antennen.

Rapportens indhold er frit tilgængeligt, men offentliggørelse (med kildeangivelse) må kun ske efter aftale med forfatterne.

Contents

Preface	xi
1 Introduction	1
2 Linkbudget	3
2.1 ADS-B signals	3
2.2 Free space loss	3
2.3 LEO coverage	4
2.4 LEO radiation pattern	5
2.5 Tabel	7
3 Antennas	9
3.1 Reflector Antennas	9
3.2 Helical Antennas	12
3.2.1 Helical antenna with ground plane	12
3.2.2 Quadrifilar Helical Antenna	16
3.2.3 Truncated Spherical Helical Antenna	23
4 Power Amplifier Imperfections	29
4.1 Amplifier non-linearity	29
4.1.1 Impact of non-linearity	31
4.2 Memory effects	33
4.3 AM/AM and AM/PM distortion	33
4.4 Crosstalk	34
4.5 Antenna Diversity and MIMO	36
5 Measurement	39
5.1 Power Amplifier	39
5.2 Measurement setup	40
5.2.1 Measurement of AM/AM distortion	42
5.2.2 PSD	44
5.2.3 ACPR	46
6 Conclusion	47

Bibliography	49
A Appendix A name	51

Todo list

Preface

Here is the preface. You should put your signatures at the end of the preface.

Aalborg University, May 6, 2019

Author 1
<username1@XX.aau.dk>

Author 2
<username2@XX.aau.dk>

Author 3
<username3@XX.aau.dk>

Chapter 1

Introduction

The goal of this project is to make an deployable antenna for Automatic dependent surveillance-broadcast (ADS-B) on a Low-Earth Orbit (LEO) satellite. ADS-B is a system in which aircraft continually transmit their identity and GPS-derived navigational information. ADS-B networks for air traffic monitoring have already been implemented in areas around the world, but ground stations cannot be installed in mid-ocean and are difficult to maintain in the Arctic, leaving a coverage gap for oceanic and high latitude airspace. Therefore a solution can be to monitor the signals with a low orbit satellite using an antenna matched to the frequencies of the ADS-B. This has already been done by the company Aireon which has 66 ADS-B receivers hosted on the new Iridium NEXT LEO satellite constellation. But this is a large satellite and a CubeSat would be better suited for the application. Therefore the antenna should fit in a 1U cubesat which can be deployed when in space.

Chapter 2

Linkbudget

2.1 ADS-B signals

There are currently three types of ADS-B transmissions but for satellite reception only the 1090 MHz extended squitter (ES) is of interest. An ADS-B message is 112 bits long and the transmission takes 120us. The modulation is Binary Pulse Position Modulation (BPPM) and the package consist of 5 parts. The first part is Downlink Format which tells that this is an ADS-B signal, second part is Additional Identifier which has different meaning within each ADS-B subtype. The third is the ICAO which is the unique identifier of the aircraft. The fourth is the DATA which contains several informations including aircraft operation status, airborne position and velocities measured from different sensors. The fifth and last is the checksum [Sun, 2015].

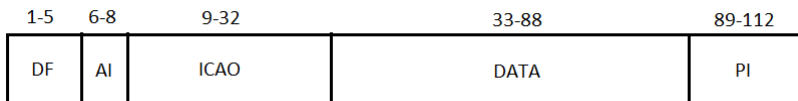


Figure 2.1: 112 bit long ADS-B message

2.2 Free space loss

Typically in satellite communication a LOS component exist. Therefore the only obstacle between the satellite and user is the atmosphere and therefore the loss can be modelled as free space, with a limited variation due to weather conditions. ADS-B signal is sent through a linear polarized monopole with power varying from 125W to 500W depending of the airplane and speed [Francis, 2011]. The height of a Low Earth Orbit (LEO) satellite is between 600 km to 800 km. To calculate the power loss Friis Transmission Equation is used.

$$\frac{P_r}{P_t} = \left(\frac{\lambda}{4\pi R}\right)^2 G_t G_r |\vec{P}_r \cdot \vec{P}_t|^2 \quad (2.1)$$

$$\lambda = \frac{c}{f} \quad (2.2)$$

Where $c = 3e8$ is speed of light in vacuum and f is the frequency in Hz. $|\vec{P}_r \cdot \vec{P}_t|^2$ denotes polarization mishmash.

2.3 LEO coverage

For a satellite the coverage area on the earth is a circular area which is defined by the height (H) of the satellite and the angle α_0 . The maximum distance the signal travels from the satellite to the earth and vice versa, is d which is depicted in figure 2.2 [Shkelzen Cakaj, 2014]. The equation for d is given by equation 2.3

$$d = R_e \left(\sqrt{\left(\frac{H + R_e}{R_e} \right)^2 - \cos^2 \epsilon_0} - \sin \epsilon_0 \right) \quad (2.3)$$

Where

$$\epsilon_0 = \arccos \frac{\sin \alpha_0 (R_e + H)}{R_e} \quad (2.4)$$

and $R_e = 6378km$ is the radius of the earth. Further the coverage percentage of the satellite can be calculated by equation 2.5 which uses the total area of the earth divided by the area covered by the satellite.

$$Coverage(\%) = \frac{A_{coverage}}{A_{earth}} = \frac{2\pi R_e^2 (1 - \cos \beta_0)}{4\pi R_e^2} \cdot 100\% \quad (2.5)$$

$$\beta_0 = 90 - \alpha_0 - \epsilon_0 \quad (2.6)$$

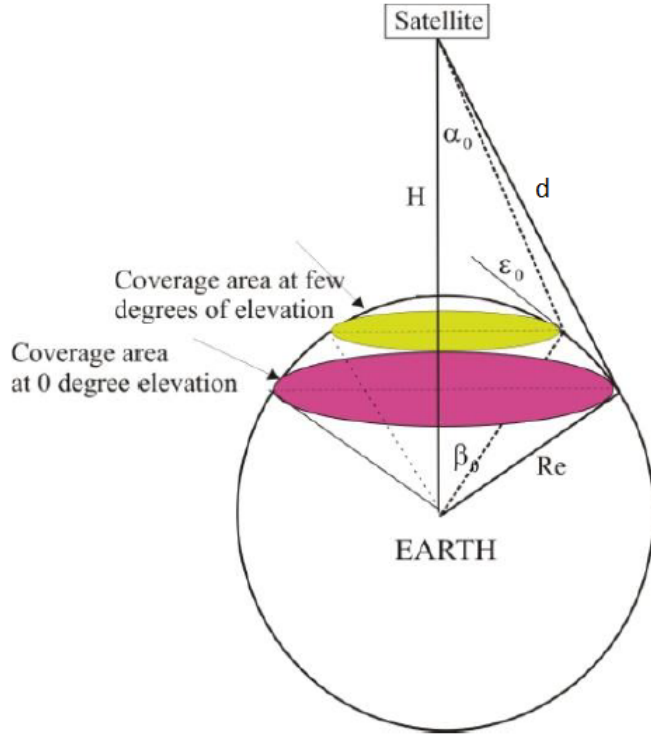


Figure 2.2: Earth coverage for a satellite. Pink area is maximum coverage, green is area limited to the antenna beamwidth. [Shkelzen Cakaj, 2014]

Because of the geometry of the earth and the height of the satellite a maximum coverage area must exist. This is depicted in figure 2.2 as purple area. To find the maximum angle of α_0 equation 2.7 is used.

$$\alpha_0(\max) = \arcsin \frac{R_e}{R_e + H} \quad (2.7)$$

2.4 LEO radiation pattern

Because of the unknown factor of which direction the signal arrives and which polarization the signal has, a circular polarized antenna is best suited for satellite communication [Balanis, 2005]. Depending on the application it can either be the ground station or satellite which polarization is circular. In this project it is desired to have the circular antenna placed at the satellite because ADS-B signals are transmitted by a linear monopole [ITU-R, 2017] attached to the top or bottom of the aircraft, depending on the size of the aircraft. As described earlier the signal does not always travel the same distance and therefore the loss is different due to the angle of reception. The farfield of the satellite antenna should therefore compensate for this by letting the gain increase due to the angle, which is depicted in figure 2.3.

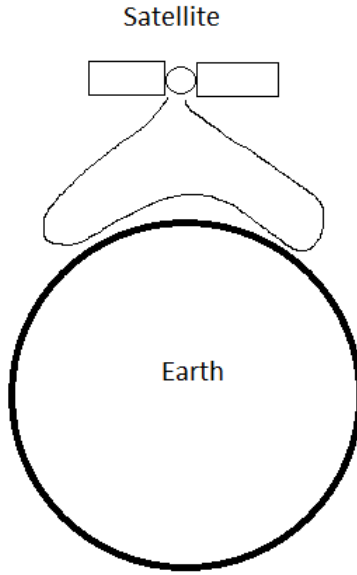


Figure 2.3: Desired farfield for a LEO satellite

Knowing equation (2.3) and (2.4) a plot of the farfield can be calculated. This is done by equation (2.8) where $d()$ is equation (2.3). The formula normalizes the gain to an angle of zero. A plot showing the relative gain at different heights is shown in figure 2.4. It is also seen from equation 2.8 that the loss due to the angle is frequency independent.

$$G_r(\alpha) = 10 \cdot \log_{10} \left(\frac{\left(\frac{\lambda}{4\pi d(0)} \right)^2}{\left(\frac{\lambda}{4\pi d(\alpha)} \right)^2} \right) = 10 \cdot \log_{10} \left(\frac{d(\alpha)^2}{d(0)^2} \right) \quad (2.8)$$

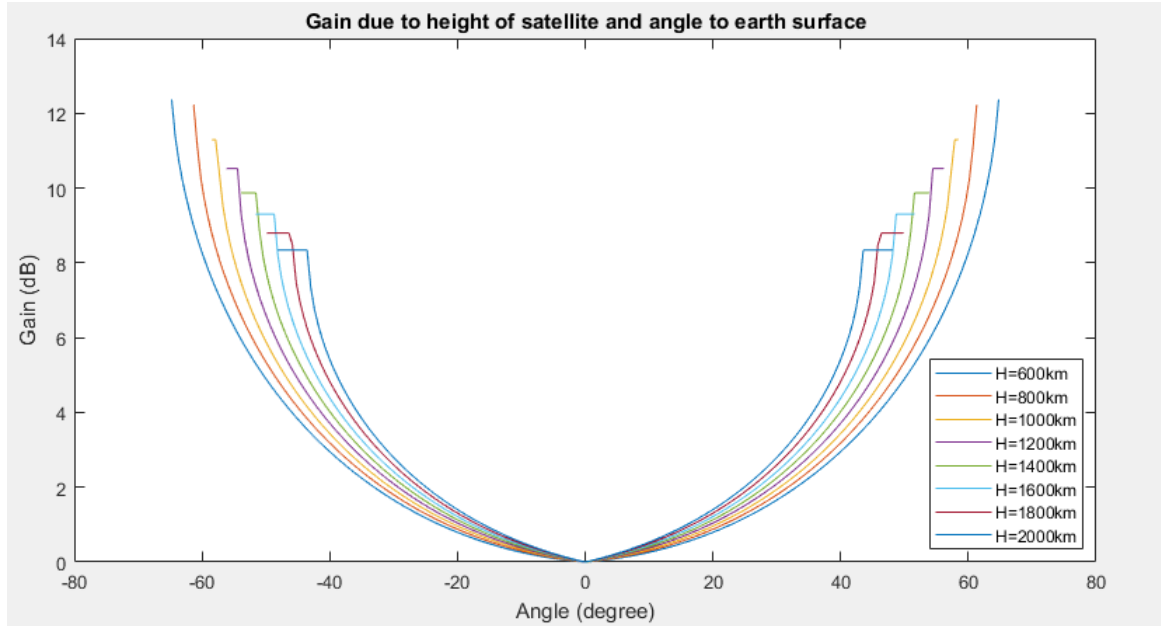


Figure 2.4: Normalized gain requirement for a LEO satellite at different heights

Table 2.1: scaling factor

Height	Max coverage	Max angle
600km	3.9%	64.7°
800km	4.9%	61.4°
1000km	5.8%	58.6°
1200km	6.7%	56.2°
1400km	7.4%	54.0°
1600km	8.1%	52.0°
1800km	8.6%	50.2°
2000km	9.1%	48.6°

2.5 Tabel

With the previously description is it now easy to calculate a linkbudget. It is assumed that the receiving antenna is a circular polarized antenna which will cause a polarization mismatch at -3dB [Balanis, 2005]. Futher an atmospheric loss at 0.1dB is assumed together with a carier to noise radio at minimum 9dB [ITU-R, 2017]. Loss due to cables or connectors has not been taken into account. The system noise temperature is set to 373K because of the high temperature span in the LEO [Francis, 2011]. The calculations is done at a transmit power at 125W and 500W which is the minimum and maximum transmit power due to the standard.

Table 2.2: Linkbudget for 1090MHZ and H = 800km

<i>Item</i>	<i>Link parameter</i>	<i>Value</i>	<i>Unit</i>	<i>Computation</i>
1	Frequency	1090	MHz	
2	Transmit power (125W)	21.0	dB	
2	Transmit power (500W)	27.0	dB	
3	Transmit antenna gain	3.0	dBi	
4	Athmospheric absorbtion (clean air)	0.1	dB	
5	Free-space loss	151.2	dB	
6	Polarisation loss	3.0	dB	
7	Received carrier power	-130.3	dB	2+3-4-5-6
8	Bandwith (4.6MHz)	66.6	dB Hz	
9	System noise temperature (373K)	25.7	dBK	
10	Boltzmann's constant	-228.6	dBW/Hz/K	
11	Noise power	-136.3	dBW	8+9+10
12	Carrier to noise ratio	6.0	db	7-11
13	C/(N+I)	9.0	db	Requirement
14	Antenna gain at 125W and $\alpha_0 = 0$	3.0	db	13-12
15	Antenna gain at 125W and $\alpha_0 = \alpha_{max}$	15.0	db	14+equation 2.7
16	Antenna gain at 500W and $\alpha_0 = 0$	-3.0	db	13-12
17	Antenna gain at 500W and $\alpha_0 = \alpha_{max}$	9.0	db	14+equation 2.7

Chapter 3

Antennas

In this section different antenna types is analysed and simulated in CST studio. Simple structures such as monopoles and dipoles is not considered since the polarization in the antennas basic form is linear. Even though it is possible to make a crossed dipole array that is circular polarized and have a high gain, but this structure would become large and still not have the opportunity to form the radiation pattern as required. Other structures such as spiral antennas and conical antennas is neither considered since those primarily is used as wideband antennas. This section will investigate the possibility to form the radiation pattern to a field to overcome the requirements from chapter 2 only.

3.1 Reflector Antennas

Reflector antennas are used places where a high gain is needed. The reflector antenna do also have a wide bandwidth, which all together has made them popular for deep space communication [William A. Imbriale, 2012]. Although reflector antennas can be made in different types, shapes and configurations, they all essentially consist of a passive reflecting surface illuminated by a smaller primary feed. The basic analysis is done using trigonometry which provides satisfactory result because the diameter of the reflecting surface often is ten times the wavelength. In figure 3.1 four main configurations is depicted. (a) is the on-focus parabolic reflector where the feed for the parabolic is placed F distance apart called the focal point. This would leave an area where the feed is placed, where there will be a gap in the coverage. This is omitted in (b) which is the off-axis reflector. This type has no gap in coverage and therefore is often used as radar. The (c) Cassegrain reflector and (d) Gregorian reflector uses both a feed in the middle of the reflector which then uses a second reflector at the focal point to reflect the energy back to the large reflector. Because of the large dimensions a reflector antenna are not suited for low frequencies $< 2\text{GHz}$. Using the equations 3.1 to 3.1 a design has been made for $f = 10\text{GHz}$, $\lambda = 30\text{mm}$, $D = 10\lambda = 300\text{mm}$, $\theta = 60^\circ$. This should give a gain at 30dBi. The design has been simulated in CST studio in figure 3.2 and 3.3. The feeding antenna used is a

dipole which is an omnidirectional antenna, this causes a loss in efficiency. An ideal reflector should be uniformly illuminated and all power should be focused on the reflecting surface. The portion of the feed power that does not reach the reflector is referred to as spillover loss while the ability to uniformly feed the parabola is referred to as illumination efficiency. Since primary feeds have a tapered radiation pattern, a compromise between spillover losses and illumination efficiency must be considered to maximize the aperture gain. In the simulation a gain at $G = 15dB$ was obtained, this could be optimized using an horn-antenna.

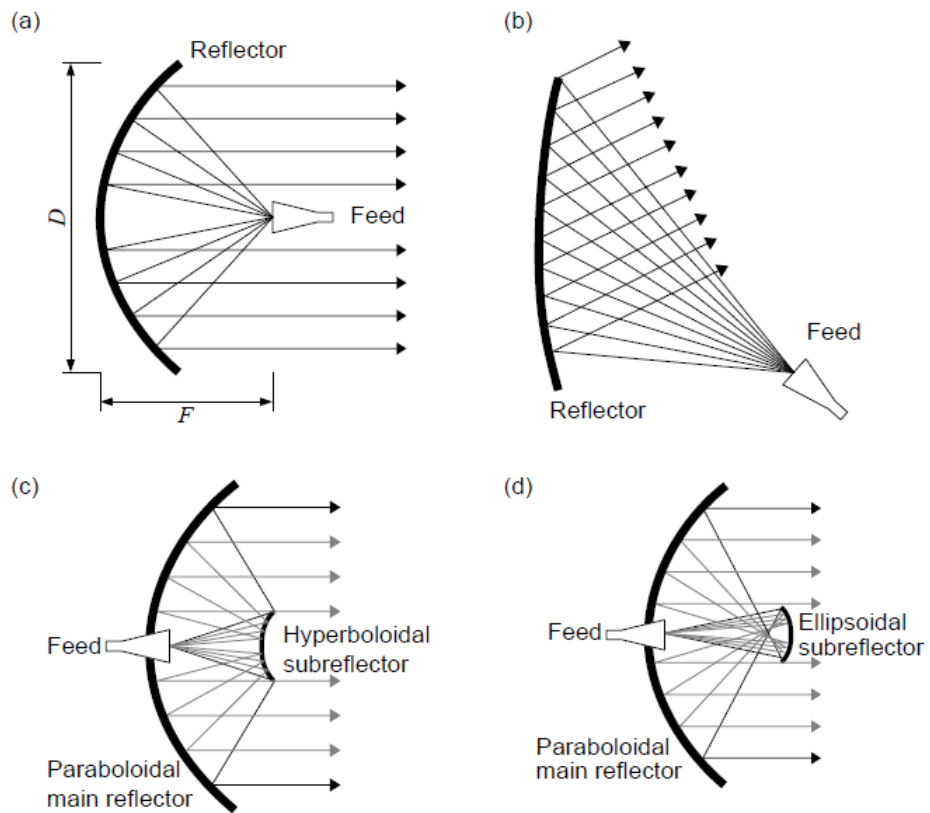


Figure 3.1: Reflector antenna configurations: (a) on-focus parabolic reflector; (b) off-axis reflector; (c) Cassegrain reflector; (d) Gregorian reflector [William A. Imbriale, 2012]

Equation for parabola

$$y = ax^2, a = \frac{1}{4F} \quad (3.1)$$

Focal length

$$F = D \frac{1}{4\tan(\theta/4)} \quad (3.2)$$

Length of parabolic segment

$$L = \frac{\ln(\sqrt{a^2 D^2 + 1} + aD)}{4a} + \frac{D\sqrt{a^2 D^2 + 1}}{4} \quad (3.3)$$

Gain for parabolic reflector

$$G = \eta \frac{4\pi A}{\lambda^2}, A = \frac{\pi D^2}{4} \quad (3.4)$$

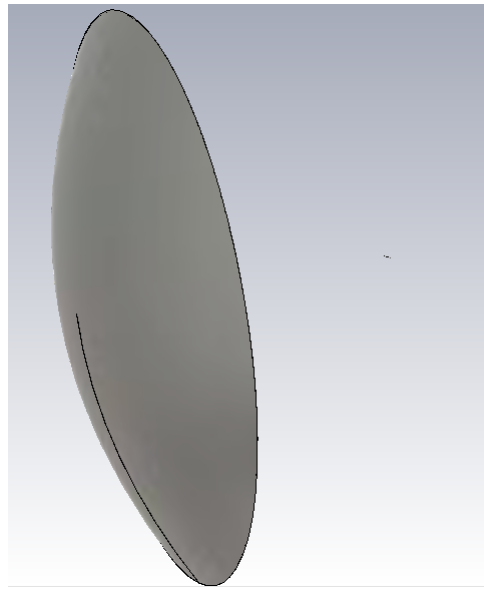


Figure 3.2: Simulated reflector antenna in CST studio

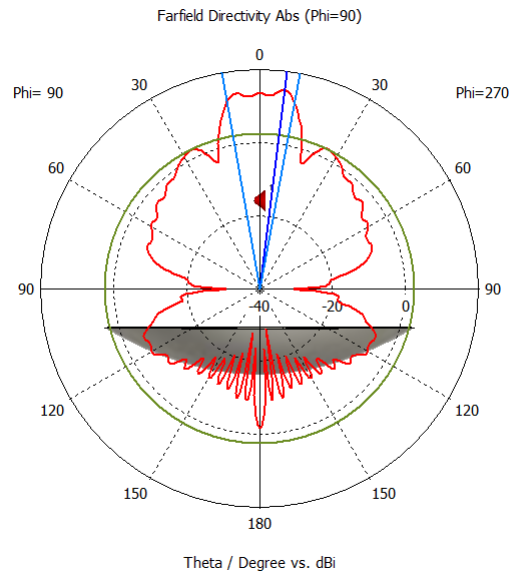


Figure 3.3: Farfield of simulated reflector antenna in CST studio

3.2 Helical Antennas

3.2.1 Helical antenna with ground plane

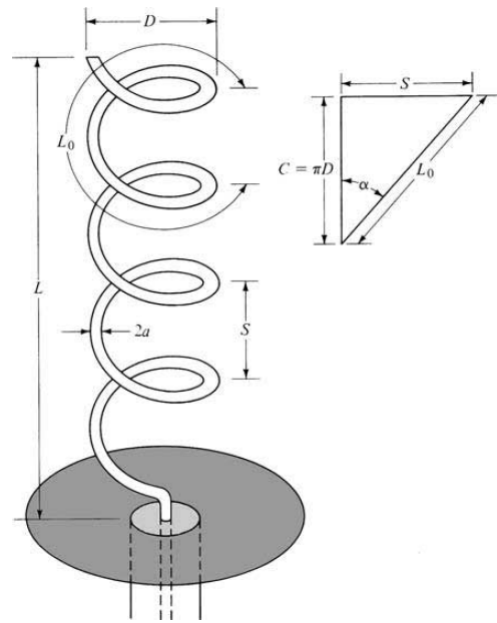


Figure 3.4: Helical antenna with ground plane [Balanis, 2005]

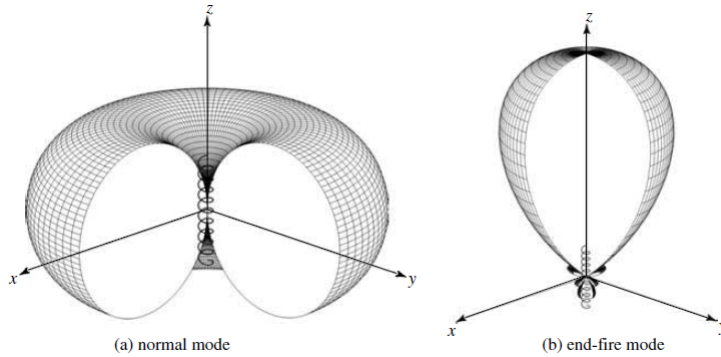


Figure 3.5: Farfield for (a) normal mode and (b) end-fire mode in linear scale [Balanis, 2005]

A helical antenna is a wire wound in form of a screw and is depicted in figure 3.4. The helical antenna consist of N turns, diameter D and spacing between the turns S and circumference is $C = \pi D$ where the total length is $L = NS$. Normally the helical antenna has a circular ground plane with the diameter $G_d = \frac{3\lambda}{4}$. Another important parameter is the pitch angle α which is the angle formed by a line tangent to the helix wire and a plane perpendicular to the helix axis. The pitch angle is defined by

$$\alpha = \tan^{-1}\left(\frac{S}{\pi D}\right) = \tan^{-1}\left(\frac{S}{C}\right) \quad (3.5)$$

The radiation pattern of the antenna can be varied by controlling the size of its geometrical properties compared to the wavelength. The input impedance is critically dependent upon the pitch angle and the size of the conducting wire, especially near the feed point, and it can be adjusted by controlling their values. The general polarization of the antenna is elliptical. However circular and linear polarizations can be achieved over different frequency ranges [Balanis, 2005]. The helical antenna can operate typically in one of two modes which is the normal (broadside) and the axial (end-fire) mode see figure 3.5. In end-fire mode a circular polarization is archived if the D and S is large fractions of the wavelength. The design criteria is $\frac{3}{4} < C/\lambda < \frac{4}{3}$ where $C = \lambda$ is optimum. $S = \frac{\lambda}{4}$ this gives a pitch angle between $12^\circ \leq \alpha \leq 14^\circ$ and a ground plane at least $G_d = \frac{\lambda}{2}$. Formulas for radiation resistance Half Power Beam Width (HPBW) and reflection coefficient is given by equation 3.2.1 to 3.2.1. The formulas has an accuracy about 20% the formulas are therefore held up with a simulation at $f = 1GHz$.

Directivity

$$D = 15N \frac{C^2 S}{\lambda^3} = 12.7dB \quad (3.6)$$

Half Power Beam Width

$$HPBW = \frac{52\lambda^{3/2}}{C\sqrt{NS}} = 46.5^\circ \quad (3.7)$$

Impedance of antenna

$$Z_l = 140 \frac{C}{\lambda} = 140\Omega \quad (3.8)$$

Reflection coefficient

$$\Gamma = \frac{Z_l + Z_s}{Z_l - Z_s} = -3.2dB \quad (3.9)$$

The simulation results are depicted in figure 3.6 to 3.8. It can be seen that the simulated results corresponds well with the formulas whit in 20% accuracy. Even though the shape of the radiation pattern can be adjusted by varying the shape of the helix, it is not possible to obtain circular polarization in those "custom" shapes and therefore the helix cannot be used for tracking of ADS-B signals other than in the end-fire mode.

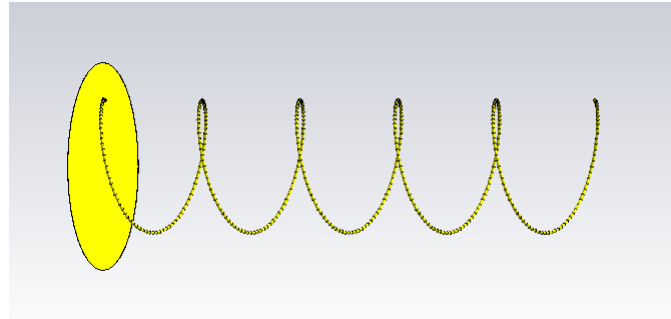


Figure 3.6: Simulated helical antenna

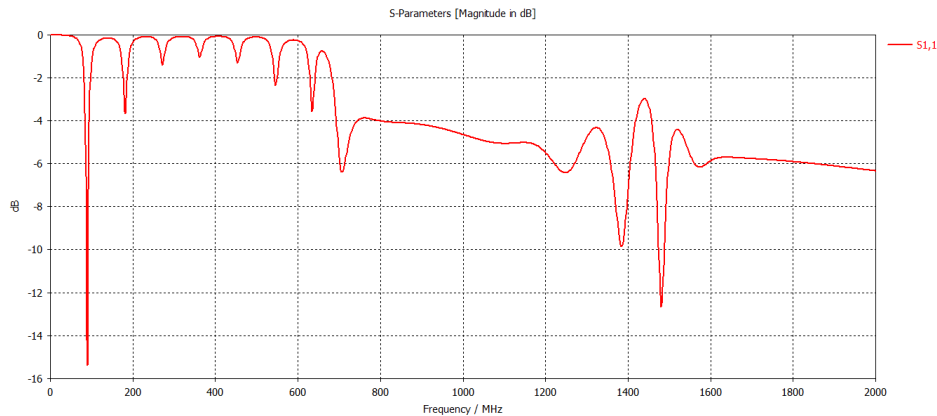


Figure 3.7: Reflection coefficient for simulated helical antenna

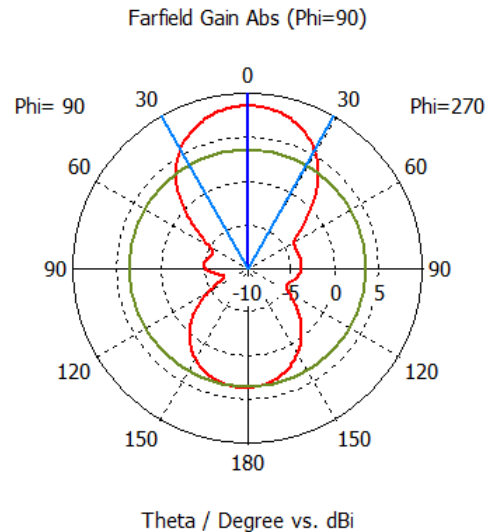


Figure 3.8: Farfield for simulated helical antenna with a maximum gain at 8.5dB and a HPBW at 58.8° . This gives a coverage percentage at the earth at 0.5%

3.2.2 Quadrifilar Helical Antenna

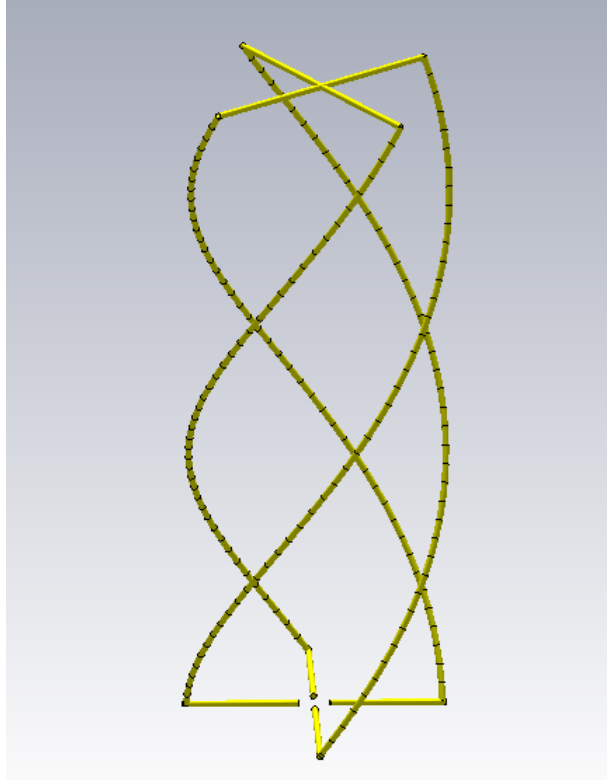


Figure 3.9: QHA with $N = 0.6$, $D = 80\text{mm}$, $L = \frac{\lambda}{2} - D \cdot 0.75$, $f = 1\text{GHz}$

The Quadrifilar Helical Antenna (QHA) (see figure 3.9) is a resonant antenna which is typically feed by two ports with a 90° phase difference. The antenna has a circular polarization and the size is often smaller than a normal helical antenna. Typically the length of each arm is an integral multiple of the quarter-wavelength. The end of the helix is open when the integer is odd, while short when the integer is even [Xudong Bai, 2014].

An QHA has been build and simulated in CST studio. The dimensions are $D = 80\text{mm}$, $L = \frac{\lambda}{2} - D \cdot 2$, $N = 0.6$ at the frequency $f = 122.5\text{MHz}$ and $\lambda = 2450\text{mm}$ with the wire diameter $Wd = 2\text{mm}$. The length is calculated so there is a half wavelength for the current flow between the negative and positive side of a port. The feeding is done using two discrete ports as shown in figure 3.10. When port 1 is fed with a positive phase at 90° the QHA will have its maximum radiation in the forward direction. If the port instead is fed with a negative phase at 90° then the QHA will have its maximum radiation in the backward direction. Other phases will result in non-uniform radiation pattern.

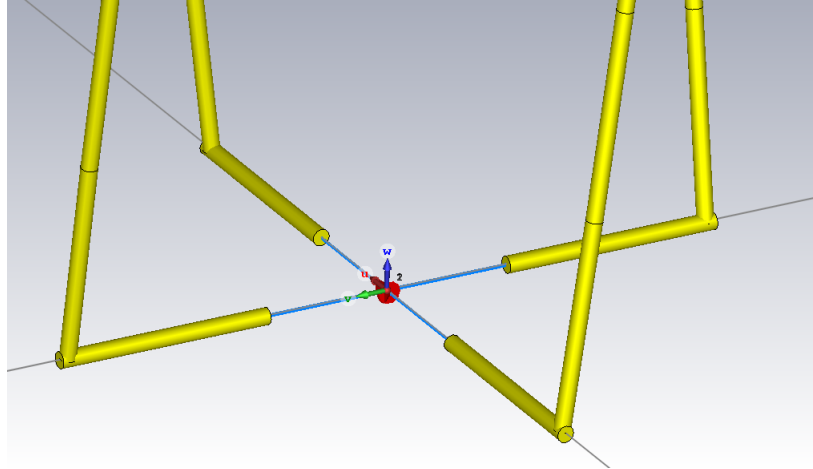


Figure 3.10: Feeding of the QHA for 122.5MHz using discrete ports

The QHA has been simulated and the results shows, that the antenna is resonating at 131MHz even thou the S11 parameter at this frequency is only -2dB, see figure 3.11. The small difference in frequency due to the calculations is caused by the gap between the ports in the bottom and the extra length caused by the turn of N. It can be seen that the antenna also radiates at multiply of the first resonant frequency and that the lowest return-loss is obtained at 4 times the frequency which gives 519MHz. The farfields for the frequencies 131,262,393 and 519MHz are shown in figure 3.12, 3.13, 3.14 and 3.15, where port 1 is fed with a positive phase at 90° . It is seen that the farfield not surprisingly changes with the frequency and that a higher frequency will result in side lobes. This could be an advantage to overcome the requirement from figure 2.3 but unfortunately the polarization becomes linear in the angle of the sidelobes which then makes this option unuseful.

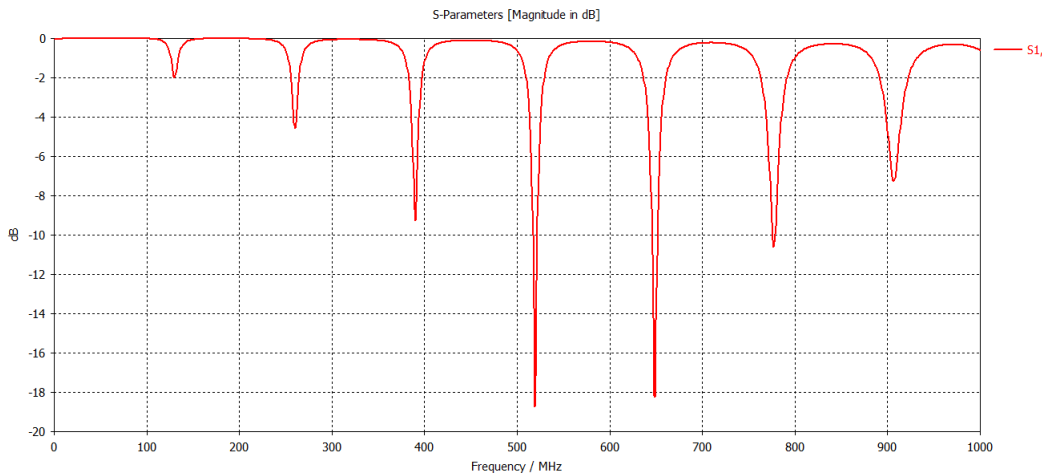


Figure 3.11: S11 parameter of the QHA for 122.5MHz

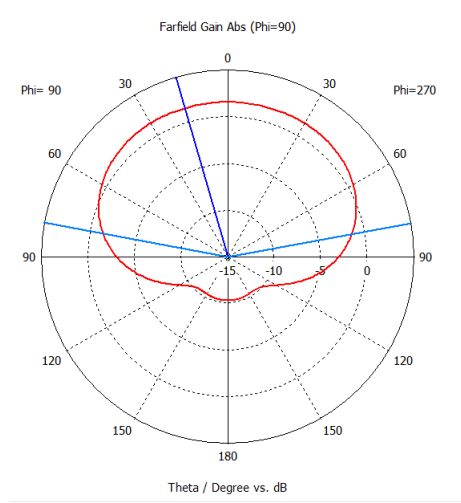


Figure 3.12: Simulated farfield at 131MHz

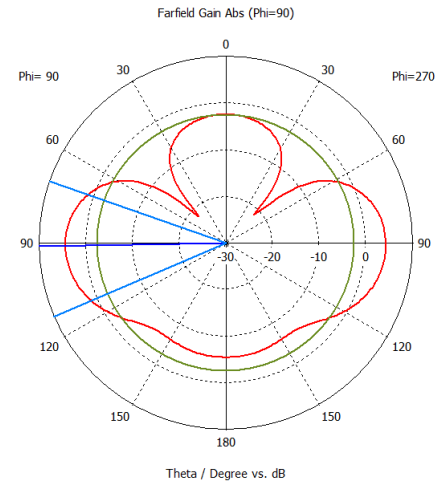


Figure 3.13: Simulated farfield at 262MHz

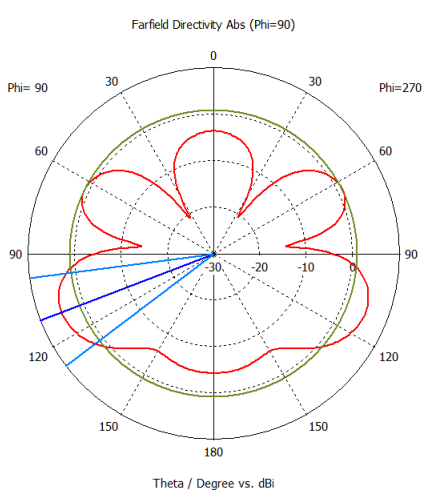


Figure 3.14: Simulated farfield at 393MHz

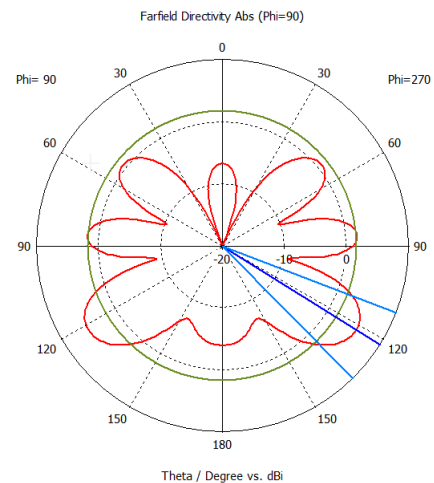


Figure 3.15: Simulated farfield at 519MHz

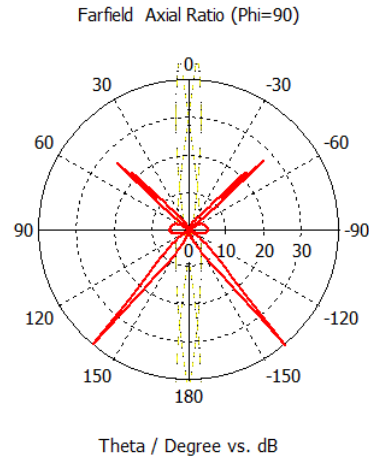
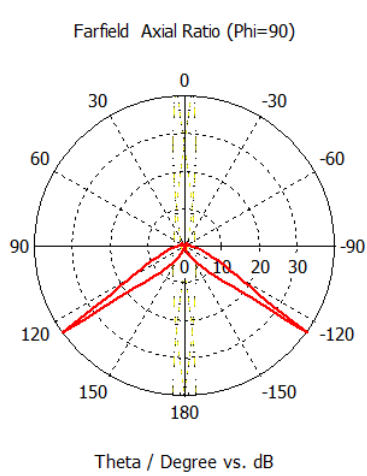
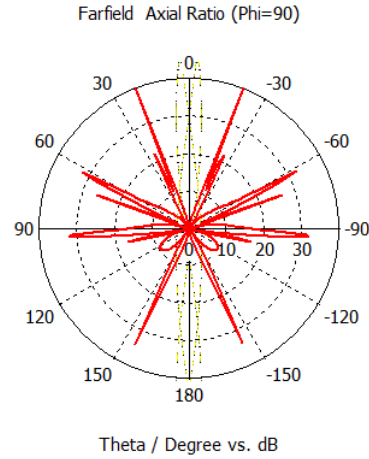
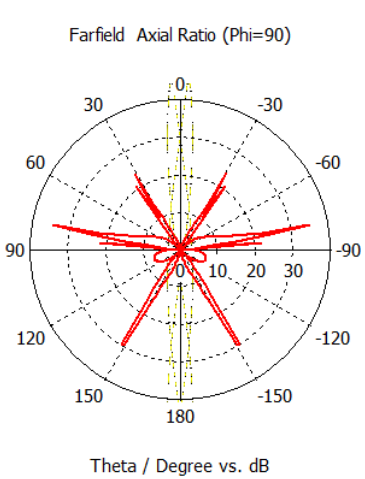


Figure 3.16: Simulated Axial Ratio at 131MHz



QHA for 1090 MHZ

By simulating the diameter of the QHA and the length, it has been shown that a diameter of $D = 0.16\lambda = 24\text{mm}$ and a length of $L = 0.22\lambda = 66\text{mm}$ gives a good performance at 1090Mhz with a S11 at -30dB. The antenna has a nearly perfect circular polarization and a maximum gain at 6.0dB together with a HPBW at 103° . This gives a coverage percentage at 1.4% on the earth at a height of 800km. The antenna has been simulated with a ground-plane and without a ground-plane and the difference in the performance is small. The feeding is done using two microstrip lines for each loop and then feeding those with a discrete port. This is done at both top and bottom of the design.

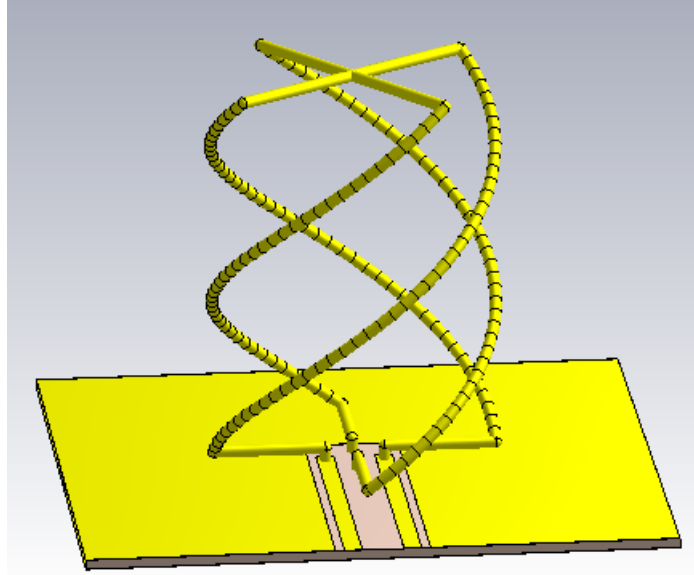


Figure 3.20: QHA for 1090Mhz with a diameter of $D = 0.16\lambda = 24mm$, a length of $L = 0.22\lambda = 66mm$ and a ground-plane at 10x10cm

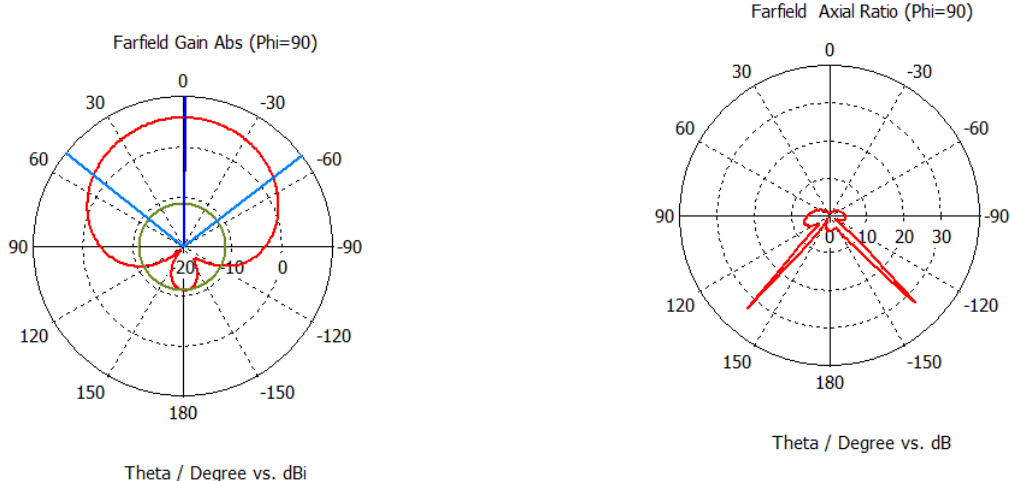


Figure 3.21: Farfield of the QHA

Figure 3.22: Axial ratio of the QHA showing good circular polarization

Wideband QHA

As shown previously a QHA in its basic form radiates only at a narrow frequency band. For the S-parameters in figure 3.11 it is seen that at 131MHz the return loss is about -2dB which results in an efficiency at only -5dB. This can be improved using a match network, but the antenna still needs to be a radiating element and therefore the matching can only improve the return-loss and not the bandwidth [Iyer,

2010]. Therefore some modifications needs to be done at the QHA to improve the bandwidth. One method is to make the bifilar arms of the QHA in different lengths so one arm is longer than the resonant frequency and the other shorter as depicted in figure 3.23. The feeding is done by shortening the feeds as in figure 3.24 and feed with a $1/4\lambda$ coax cable as balun. Because the feeding is done this way the farfield will not be omnidirectional and is skewed in one direction as depicted in figure 3.25. A more omnidirectional radiation pattern could be obtained by looking more into the feeding method. It has been shown in [Xudong Bai, 2014] that it is possible to use a feeding network consisting of one second-iteration Moore 180° hybrid coupler and two second-iteration Sierpinski 90° hybrid couplers. It has also been shown in [Xiaoqiang Yang, 2014] that a broadband feed network can be done using an wilkinson powerdivider and broadband 90° phase shifters.

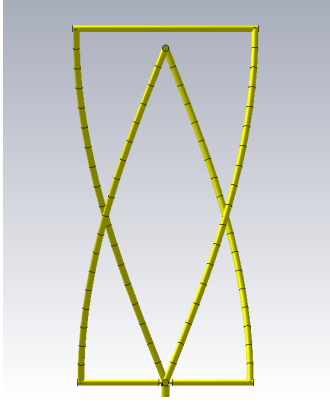


Figure 3.23: Wideband QHA with dimensions
 $f = 1GHz$, $\lambda = 300mm$, $R1 = \lambda 0.091$, $L = \lambda 0.36$,
 $R2 = \lambda 0.086$, $L = \lambda 0.34$

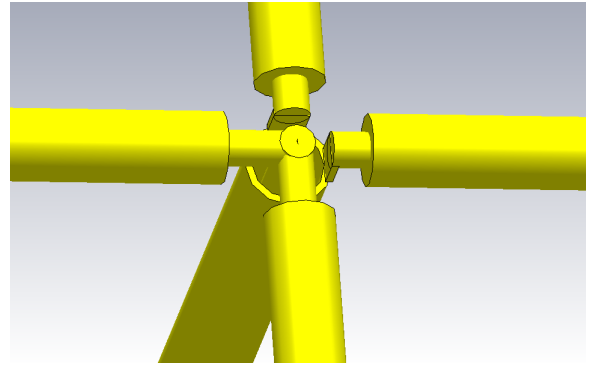


Figure 3.24: Feeding for the wideband QHA

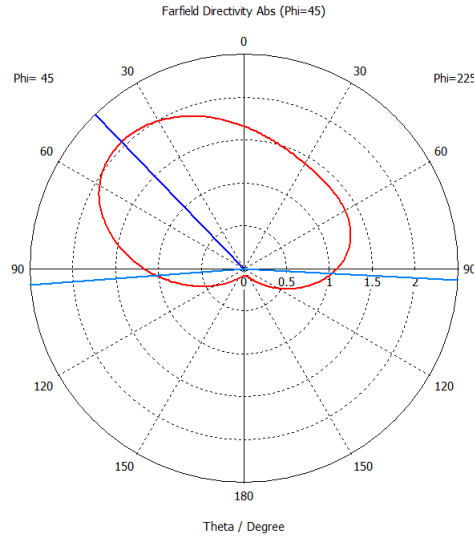


Figure 3.25: Farfield for the wide band QHA in linear scale

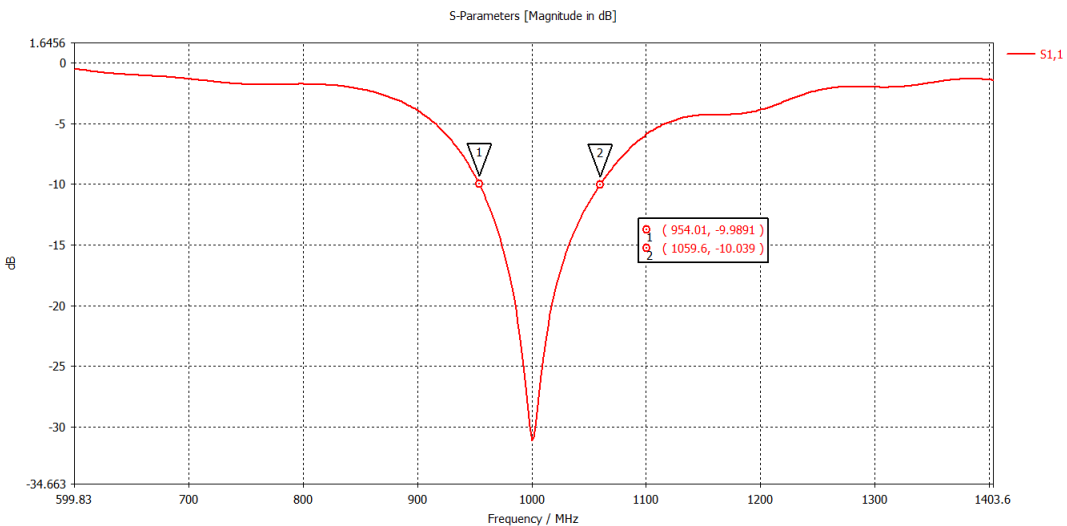


Figure 3.26: S-parameters for the wideband QHA shows a bandwidth at 10%

Multiband QHA

Another configuration of the QHA is the Multiband QHA [Xudong Bai, 2014] which can be build up on several narrowband or wideband QHA's inside each other as depicted in figure 3.27. This configuration allows several frequency bands to be covered since several QHA's can be build inside each other. The consequence is though a heavy and complex design which may also needs a complicated feeding network or several ports for each frequency.

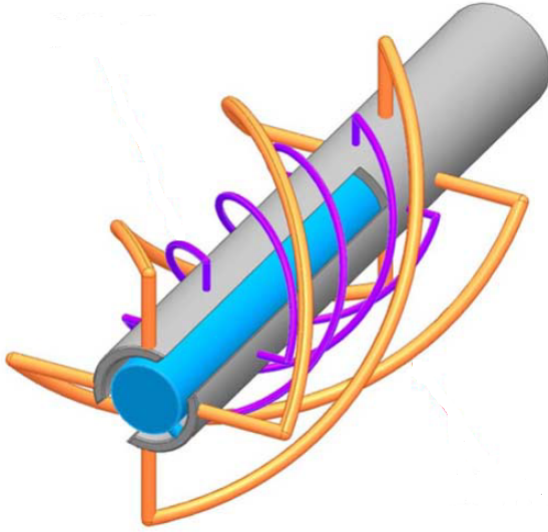


Figure 3.27: Dual band QHA using two single QHA's [Xudong Bai, 2014]

3.2.3 Truncated Spherical Helical Antenna

The Bifilar Truncated Spherical Helical Antenna (BTSHA) is a modification of the normal Spherical Helical Antenna (SHA) whose geometry is described by equation 3.10 to 3.12 in spherical coordinates, where N is number of turns of the wire. The BTSHA is made upon two half's of the SHA which then is turned 180° to connect to each other. See figure 3.28.

$$r = a \quad (3.10)$$

$$\theta = \cos^{-1}\left(\frac{\phi}{N\pi} - 1\right) \quad (3.11)$$

$$0 \leq \phi \leq 2\pi N \quad (3.12)$$

The BTSHA can be fed different ways using bottom feeding, side feeding or top feeding. One advantage using top feeding is that it can be fed using a "monopole" that will make a field inside the BTSHA together with the current flowing in opposite direction which makes it able to radiate in axial-null mode because of the symmetry. See figure 3.29. This makes it possible to archive better gain in the side direction as wanted for a satellite antenna for reception of ADS-B. Unfortunately the structure has a lack of gain in the center which would result in no reception in the direct path to the earth. A solution for this has to be found. Another advantage is the compact size compared to a conventional helical antenna. An important feature of this structure is that the angle of the cone can be adjusted by moving the height of

the ground-plane. If the cone shall become broader the ground plane can be moved backward and if the cone is wanted narrower then the ground plane can be formed as an reflector. Simulations has shown that the number of the wire turns has only little effect on the S-parameter and radiation pattern. A simulation has been made with the dimension $a = 2.86\lambda$, see figure 3.30. It is stated in [Clark, 2003] that the radiation pattern for this dimension should be omnidirectional. This has been shown not to be fully true and there is only two main-beams. The polarization is overall circular but with linear polarization in the direction of the two main-beams.

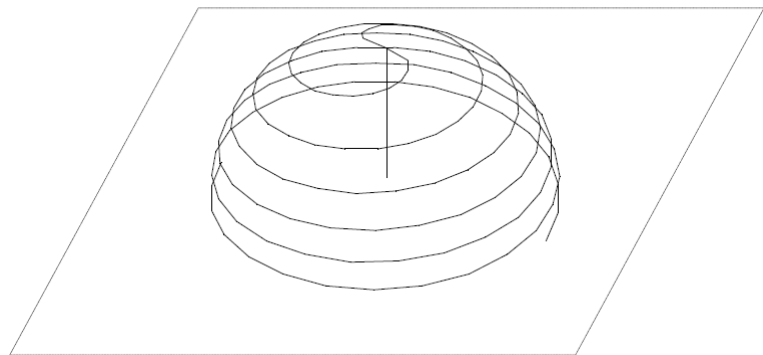


Figure 3.28: Bifilar Truncated Spherical Helical Antenna [Clark, 2003]

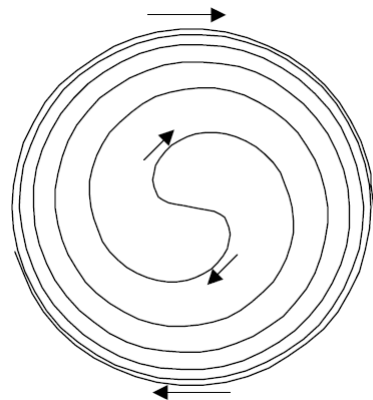


Figure 3.29: Currentflow of the BTSHA [Clark, 2003]

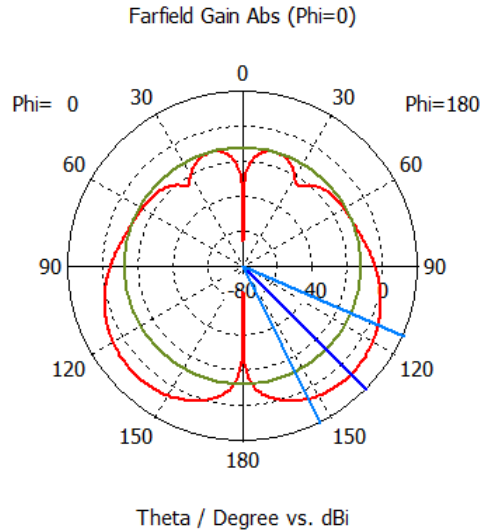


Figure 3.30: Farfield of a simulated BTSHA with $a = 2.86\lambda$ and $N = 1.5$. Maximal gain is 7.1dB. Be aware that the structure at only this farfield is pointing at 180°

Another simulation has been shown to have a more omnidirectional radiation pattern, which uses four arms instead of two (QTSHA) with a rotation of 90° each. Further the structure is stretched in the Z-direction by a factor of two. The stretching gives a higher gain and a broader radiation angle close to 100° , but still this structure has a lack of gain in the center and the polarization becomes non circular. To overcome this problem simulations has shown that it is rather difficult to make a change to the structure that will increase the gain in the middle. The best solution to this problem is to change the feed point, see figure 3.33. The feeding point has been simulated for various points and a feeding point at 0.06λ from the top has shown to be the best. See figure 3.34. Unfortunately this does not help making the structure circular polarized.

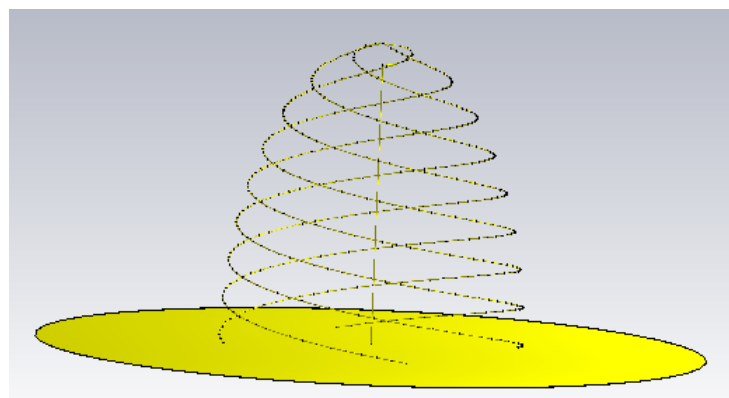


Figure 3.31: Stretched Quadrifilar Truncated Spherical Helical Antenna

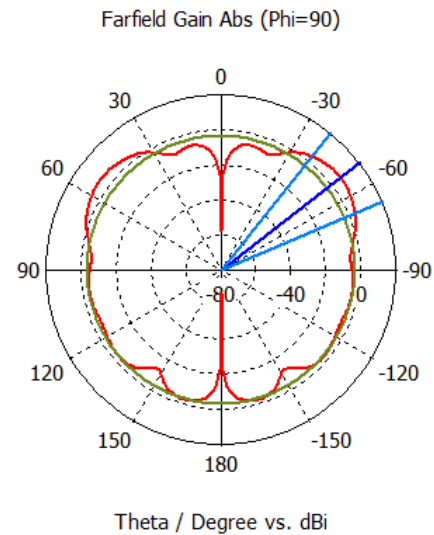


Figure 3.32: Farfield of a simulated QTSHA with $a = 2.86\lambda$ and $N = 1.5$. Maximal gain is 5.9dB

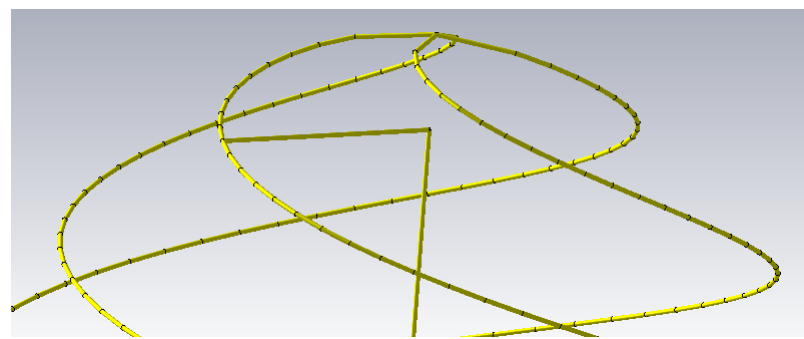


Figure 3.33: Position of the changed feeding point

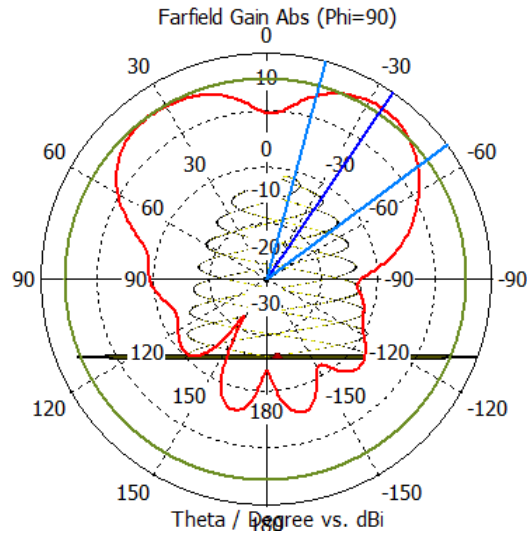


Figure 3.34: Farfield of a simulated QTSWA with $a = 2.86\lambda$ and $N = 1.5$. The figure is fully omnidirectional.

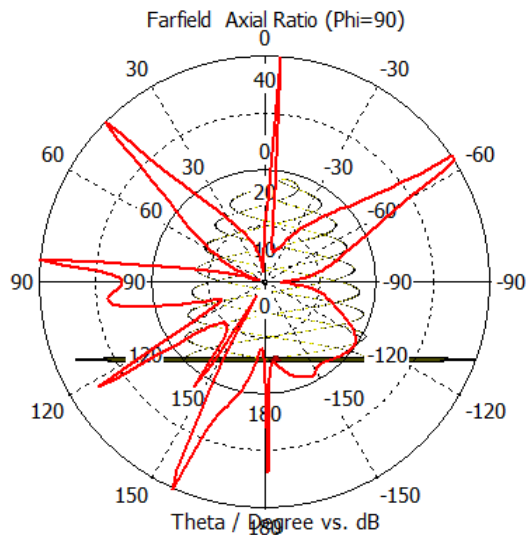


Figure 3.35: Axial ratio of the simulates antenna shows that this is not a circular polarized antenna

Chapter 4

Power Amplifier Imperfections

4.1 Amplifier non-linearity

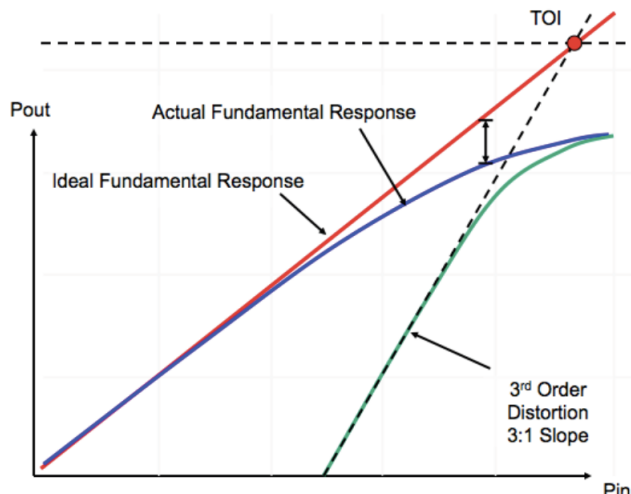


Figure 4.1: Amplifier non-linearity [National-Instruments, 2019]

A power amplifier (PA) has a voltage-in to voltage-out relationship that can be described by the figure depicted in 4.1 as actual fundamental response. This causes a distortion at the output which can be described by equation 4.1 [National-Instruments, 2019].

$$V_{out} = a_0 + a_1 V_{in} + a_2 V_{in}^2 + a_3 V_{in}^3 + a_4 V_{in}^4 + \dots \quad (4.1)$$

Where V_{out} is the output signal from the amplifier, $a_1, a_2, a_3..$ is coefficients describing the ratio of the distortion and V_{in} is the input. If a single tone input is presented, then the output will consist of purely odd and even harmonic distortion. If a input-signal using two tones is considered then there will be a difference and a

sum of the frequencies presented at the output which is caused by the cubic term in equation 4.3. This is also called Two-Tone Third-Order Intermodulation Distortion and is also depicted in figure 4.1 as 3rd order distortion with a slope of 3:1. It can be seen that when the output power increases then the distortion increases 3 times. A measurement of this is called the third-order-intercept-point (IP3 or TOI). However, the intersection is fictitious it is realized only in mathematics and used as a figure of merit in industry. It can be seen from figure 4.2 that the distorted component are spaced too close in frequency to be effectively filtered, which would need an other technique to be removed. Such a technique could be Digital Pre-Distortion (DPD)

$$V_{in} = \sin(\omega_1 t) + \sin(\omega_2 t) \quad (4.2)$$

$$V_{out} = a_0 + a_1(\sin(\omega_1 t) + \sin(\omega_2 t)) + a_2(\sin(\omega_1 t) + \sin(\omega_2 t))^2 + a_3(\sin(\omega_1 t) + \sin(\omega_2 t))^3 + \dots \quad (4.3)$$

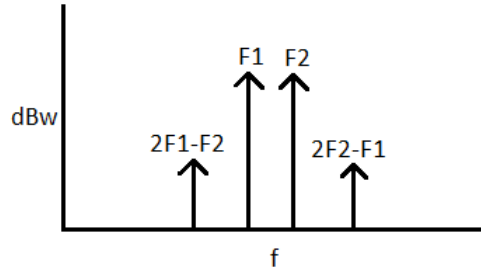


Figure 4.2: Two-Tone Third-Order Intermodulation Distortion

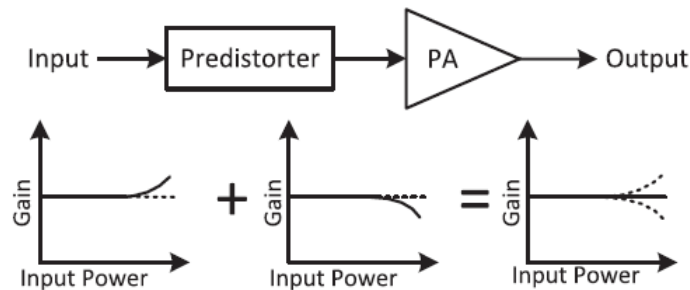


Figure 4.3: Concept of predistortion [Yan Guo, 2015]

In figure 4.6 the concept of DPD is depicted. DPD is a way to "distort" the incoming signal with the inverse transfer-function of the amplifier. For example the gain of the amplifier is ideally linear in the small-signal region and gets non-linear at higher signal levels. To overcome this, a block called the predistorter inverses this

non-linear curve which is the exact inverse of the PA, then a linear amplification can be achieved at the final PA output. But to archive this exat inverse of the PA all the non-linear effects has to be accounted for.

4.1.1 Impact of non-linearity

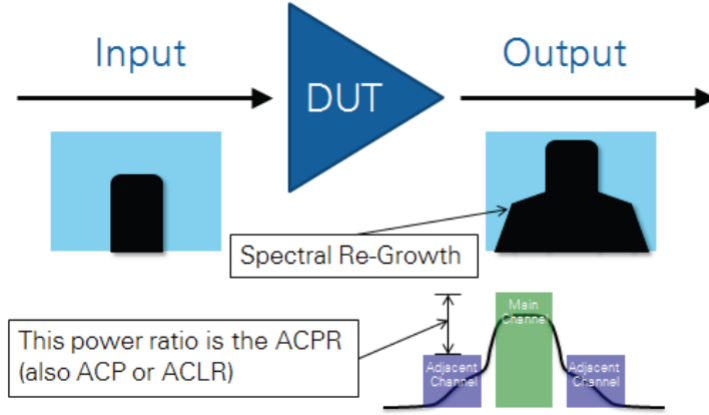


Figure 4.4: Graphical Depiction of ACPR in the frequency domain [National-Instruments, 2019]

Due to the imperfections of the PA spectral regrowth will occur which will affect nearby channels. The Adjacent Channel Power Ratio (ACPR) is a measure of the power of the distortion components, caused by the non-linearity of the PA, that are leaked into the adjacent channel see figure 4.4. The formula for the ACPR is given by equation 4.4 and is used after a Fourier transform has been performed at the output of the PA.

$$ACPR = \frac{\int_{adjch} |Y(f)|^2 df}{\int_{mainch} |Y(f)|^2 df} \quad (4.4)$$

Where $Y(f)$ is the Fourier transform of the signal, adjch is the adjacent-channel and mainch is the main-channel.

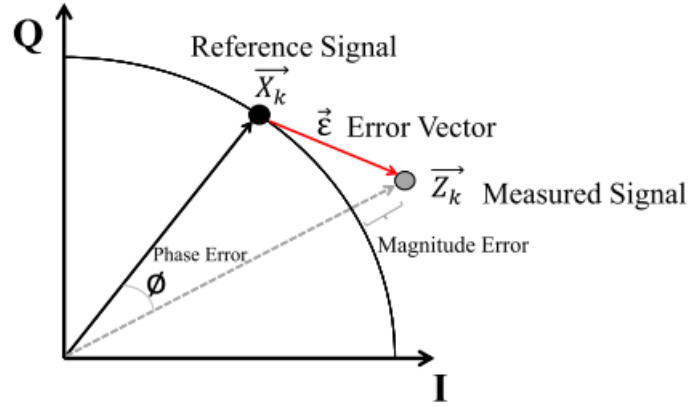


Figure 4.5: Graphical view of the EVM

Another measure of the error is the Error Vector Measurement (EVM) or Relative Constellation Error (RCE) which both is a measure of the error due to the constellations points in a IQ plot. If a signal is sent through an amplifier with a given IQ value, then the amplifier will distort those IQ values. The EVM and RCE is a measure of the power of the error vector divided by the power of the reference vector. [Ali Cheaito, 2016]

$$EVM = \frac{P_{error}}{P_{reference}} = \frac{E[|z(t) - x(t)|^2]}{E[|x(t)|^2]} \quad (4.5)$$

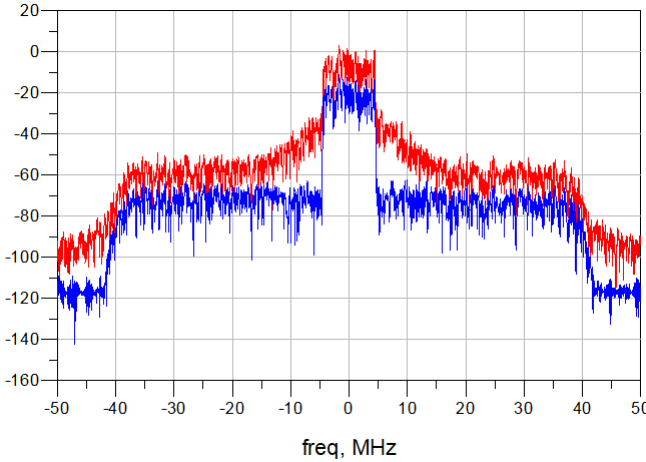


Figure 4.6: Distortion simulated in ADS, where blue is input-signal and red is output-signal. The simulation is made with a single amplifier connected to a 50Ω resistor. It is clearly that the output-signal is distorted.

4.2 Memory effects

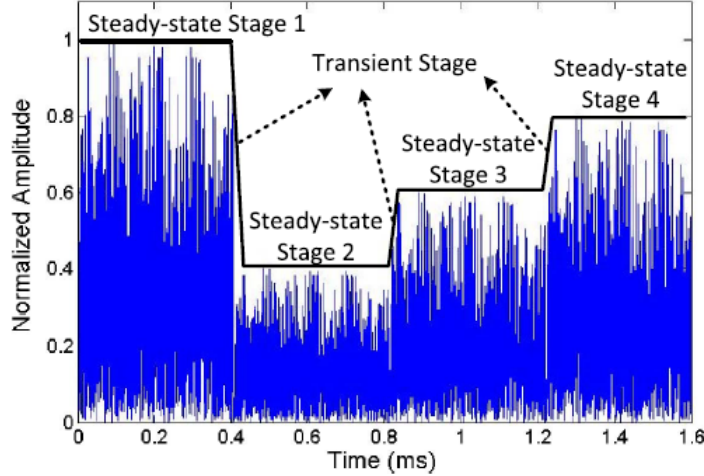


Figure 4.7: Amplitude changes at the input of the PA [Yan Guo, 2015]

In modern communication systems, the input power to the PA may be adjusted corresponding to the needs by the network. This makes a suddenly increase or decrease in the power as depicted in figure 4.7 which makes the PA work in the transient stage. The stages of the PA can be divided into two stages, where, 1) Transient stage: The period when the input power of the PA jumps from one level to another and 2) the steady-state stage: the period when the average input power level is fixed [Yan Guo, 2015]. In [Taijun Liu, 2007] memory effects is defined as following: *Memory effects can generally be classified as electro-thermal memory effects and electrical memory effects. The electro-thermal memory effects are mainly caused by the thermal capacitance and resistance that form a low pass thermal filter. The electrical memory effects can be mainly attributed to the non-constant frequency response of the PA around the carrier frequency, the impedance variation of bias circuits at baseband, and the harmonic loading in the PA power stage.* Even modelling of this is rather comprehensive the DPD still needs to take these effects into account to generate a non-distorted output at the PA.

4.3 AM/AM and AM/PM distortion

If the input signal to the PA is modelled as equation 4.6

$$x(t) = a(t)e^{j\phi(t)} \quad (4.6)$$

Where $a(t)$ is the envelope of the signal and $e^{j\phi(t)}$ is the phase of the input signal. Then the distorted output of the amplifier will be that of equation 4.6 where

$g()$ is the amplitude distortion and $f()$ is the phase distortion also called Amplitude to Amplitude (AM/AM) and Amplitude to Phase (AM/PM) distortion. AM/AM distortion can be defined as the deviation from the constant gain when PA is operated in compression region. On the other hand, the increased phase change at compression region can be termed as AM/PM distortion. In presence of wideband signals having non constant amplitude, PA behaves as nonlinear system and exhibits two types of nonlinearities which is static distortion and memory effects.

$$y(t) = g(a(t))e^{j\phi(t)+f(a(t))} \quad (4.7)$$

4.4 Crosstalk

Crosstalk is coupling from one branch to another branch. When only a signal is present on a single branch, no crosstalk would appear to this branch. On the other hand if a signal is presented at two branches then crosstalk would appear to both of them. There exist three types of crosstalk where 1) Crosstalk before the PA's, see figure 4.8, 2) Crosstalk after the PA's, see figure 4.9. 3) Crosstalk on the antennas and mishmash due to coupling. Crosstalk before the PA is also called nonlinear since it is amplified by the non linear PA. The nonlinear crosstalk and the PA nonlinear response should be jointly compensated by a predistorter to get a reliable system performance [Zahidul Islam Shahin, 2017] denoted $\mu_k()$. The output from the branches would become that of equation 4.8.

$$Y_{1k} = fk(uk(X_{11}, X_{12}, X_{13}, X_{1k})) \quad (4.8)$$

Where X is the input signal, Y is the output and fk is the PA response.

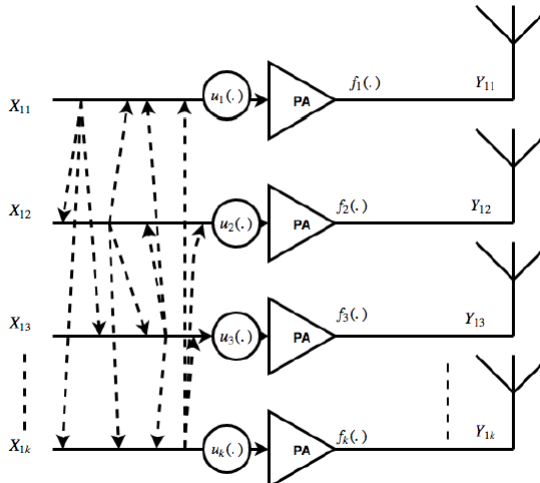


Figure 4.8: Crosstalk before PA [Zahidul Islam Shahin, 2017]

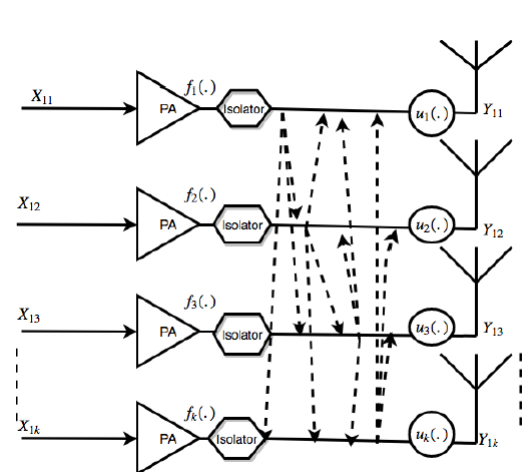


Figure 4.9: Crosstalk after PA [Zahidul Islam Shahin, 2017]

Crosstalk after the PA is called linear since it has an linear impact. In figure 4.9 the output of the amplifier is connected to an isolator, which makes the output unaffected by reflections. A linear model can therefore be used which is shown in equation 4.9.

$$Y_{1k} = \mu_k(f1(X_{11}), f2(X_{12}), f3(X_{13})..fk(X_{1k})) \quad (4.9)$$

When no isolators is presented the output will now be affected by the crosstalk or mutual-coupling between the antennas. A sketch of this is depicted in figure 4.10 where a_{1k} is the incoming signal to the amplifier, b_{2k} is the output from the amplifier and a_{2k} is the reflected signal form the antenna array at the k'th branch [Katharina Hausmair, 2017]. The relation between a_{2k} and the output signals b_{2k} is determined by the characteristics of the antenna array. The system model of the multi-antenna transmitter can, therefore, be split in to a crosstalk and mismatch model (CTMM). This block can further be used together with a dual-input-DPD which holds the model for the PA, see figure 4.11.

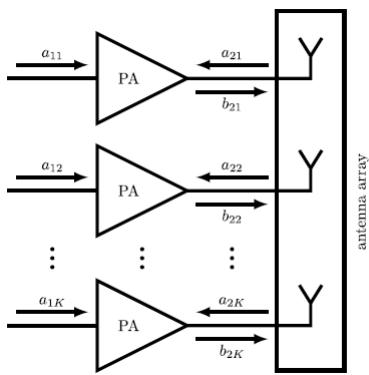


Figure 4.10: Model of the antenna crosstalk [Katharina Hausmair, 2017]

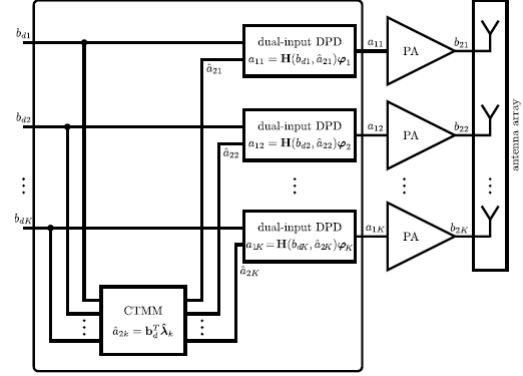


Figure 4.11: The predistortion method consists of two main blocks: one linear CTMM block for the whole transmitter and a dual-input DPD block in every transmit path. [Katharina Hausmair, 2017]

4.5 Antenna Diversity and MIMO

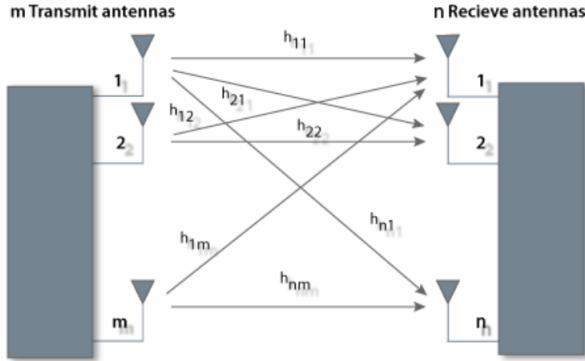


Figure 4.12: Concept of mimo

MIMO (Multiple Input Multiple Output) systems are systems with Multiple Element Antennas at both link ends. The antenna elements of a MIMO system can be used for four different purposes: beamforming, diversity, interference suppression, and spatial multiplexing which is transmission of several data streams in parallel that allows improvement of capacity. A MIMO system is modelled as in equation 4.10 and is also depicted in figure 4.12.

$$\mathbf{y} = \mathbf{H}\mathbf{x} + \mathbf{n} \quad (4.10)$$

Where \mathbf{y} is the received vector, \mathbf{H} is the channel matrix, \mathbf{x} is the transmitted vector and \mathbf{n} is noise. If the full channel matrix is known then the transmitted vector can be obtained by the receiver like equation 4.11.

$$\mathbf{x} + \mathbf{n} = \mathbf{H}^1\mathbf{y} \quad (4.11)$$

The principle of MIMO is to ensure that the same information reaches the receiver on several statistically independent channels. In MIMO systems, several transmits paths is archived by use of several antennas, which gives a spatial separation if they are separated enough to give a correlation factor ρ that is below 0.5 – 0.7 [Molisch, 2011]. The formula for the envelope correlation factor between two antennas is given by equation 4.12. The formula assumes that the WSSUS (Wide-Sense Stationary Uncorrelated Scattering) model is valid, no LOS exists, the power delay profile has an exponential shape, the incident power is isotropically distributed in azimuth and only propagates in the horizontal plane, and an omni-antenna is used.

$$\rho = \frac{J_0^2(k_0 v \tau)}{1 + (2\pi)^2 S_\tau^2(f_2 - f_1)^2} \quad (4.12)$$

Where J_0 is the Bessel function of the first kind and S_τ is the delay-spread of the channels. If the correlation between two antennas is investigated for the same frequency, then the formula can be rewritten as equation 4.13 because $f2 - f1 = 0$.

$$\rho = J_0^2(2\pi d)^{-1} \quad (4.13)$$

Where d is the element spacing given in wavelengths. A plot of this can bee seen in figure 4.14.

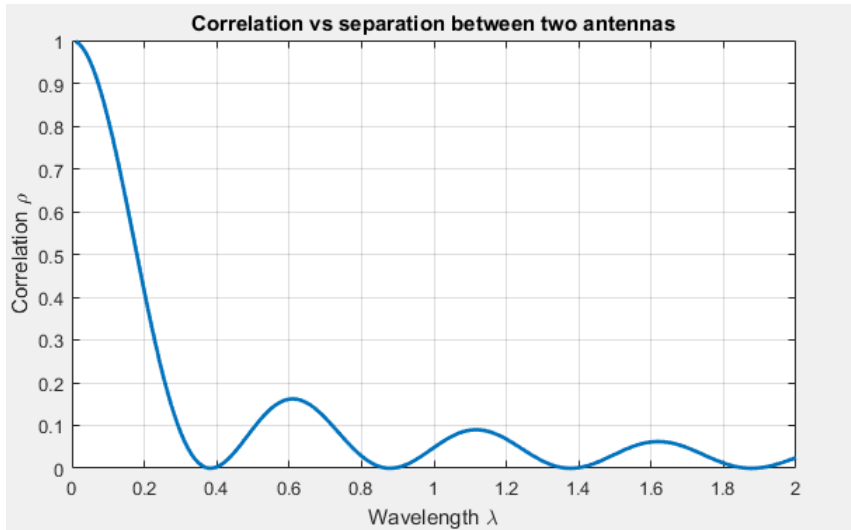


Figure 4.13: Correlation factor for two antennas versus distance

Another method to calculate the correlation factor is to use measured or simulated S-parameters as shown in equation 4.14 [Xuan Wang, 2011] where k is the propagation constant and d the distance in meters.

$$\rho = \frac{A + BJ_0(kd)}{B + AJ_0(kd)} \quad (4.14)$$

$$A = -2Re(S_{12}^*(1 - S_{11})) \quad (4.15)$$

$$B = |1 - S_{11}|^2 + |S_{12}|^2 \quad (4.16)$$

A simulation has been made in CST studio with 4 antennas separated 0.1λ at $f = 3.5Ghz$ or 8.6mm, see figure 4.14. The simulated S-parameters has been imported to MATLAB and the formula is used to generate the correlation plot in figure 4.15. From the figure it can bee seen that when the frequency increases the correlation becomes lower.

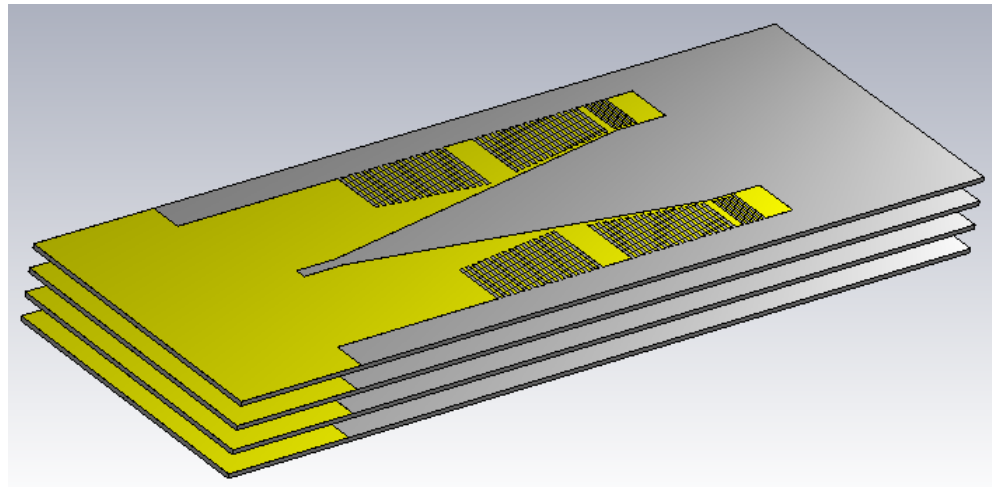


Figure 4.14: 4 wideband PCB antennas separated 8.6mm

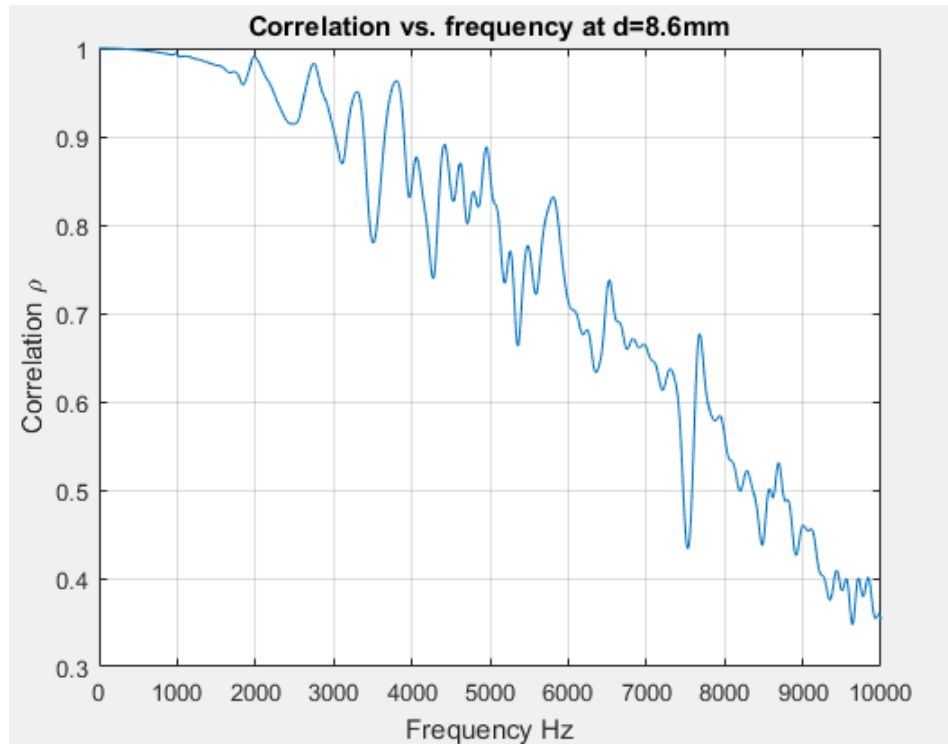


Figure 4.15: Correlation between antenna 1 and 2

Chapter 5

Measurement

The purpose of this section is to characterize a power amplifier for its distortion mechanisms and then measure the impact of the crosstalk from the antennas.

5.1 Power Amplifier

The *ZX60-6013E+* amplifier is a small buffer-amplifier with a BW from 20MHz - 6GHz. It has an output-power at maximum 11.16dBm at 3.5GHz (1 dB compression). The gain is 13.85 dB and the noise figure is 3.42dB. In figure 5.2 and 5.3 curves for the amplifier gain and output power versus frequency it depicted respectively. The amplifier is shown in figure 5.1



Figure 5.1: The *ZX60-6013E+* amplifier

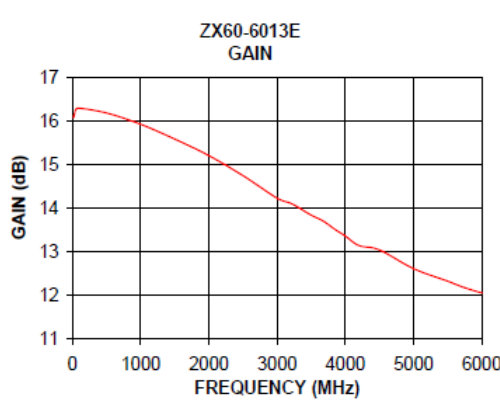


Figure 5.2: Gain versus frequency

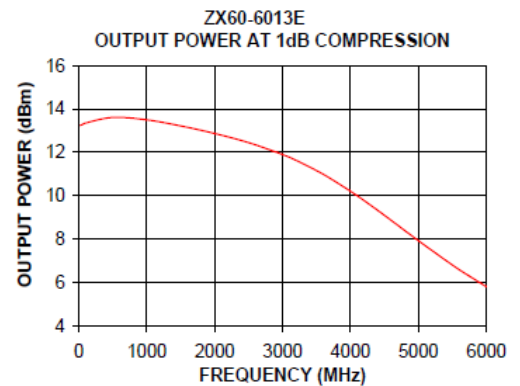


Figure 5.3: Output power versus frequency

5.2 Measurement setup

To measure the impact of the antenna crosstalk, several measurements must be done at different setup. The first setup is shown in figure 5.4. In this setup only the amplifier is measured because it is necessary with a reference. The signal generator is generating a 10MHz LTE signal at 3.5GHz which output is then connected to the input of the amplifier. The amplifier is supplied with a 12.0VDC signal from the power supply and the output of the amplifier is connected to a 6dB attenuator to protect the input stage of the spectrum analyser, which measures the output signal from the amplifier.

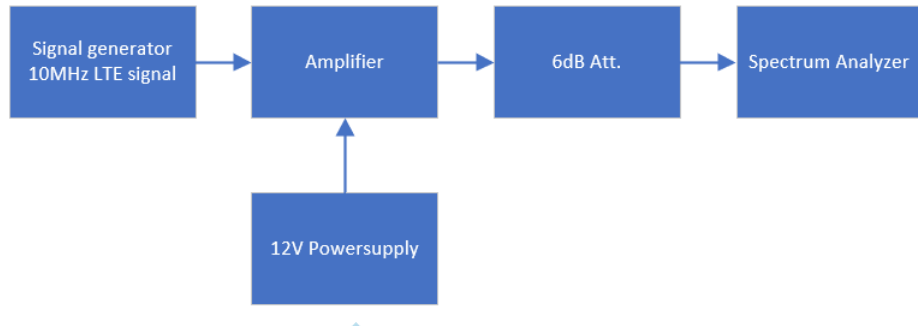


Figure 5.4: Block diagram of measurement at amplifier

In figure 5.5 the second measurement setup is shown. In this setup the antennas are now introduced. The Tx antenna is connected to the output of the amplifier. The Rx antenna are spaced 1 meter apart from the Tx antenna (measured from feed to feed). The 6dB attenuator is removed and the antenna is connected to the spectrum analyzer.

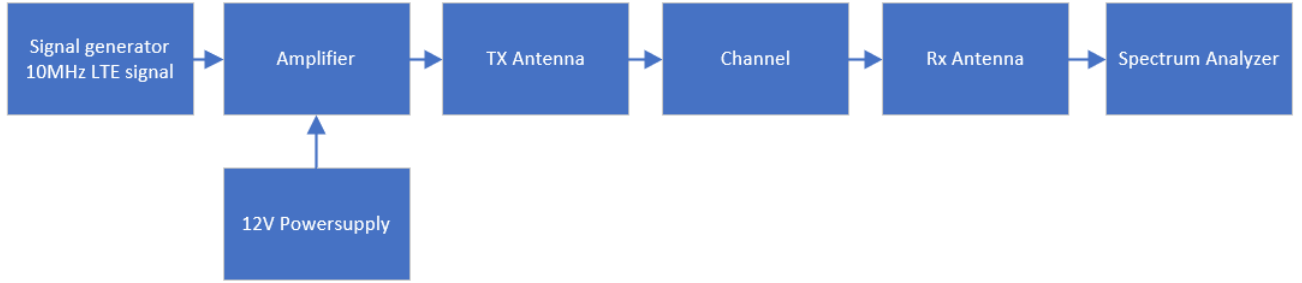


Figure 5.5: Block diagram of measurement using one antenna

In setup three a power-divider is now introduced together with a second amplifier and another antenna. The received power will now increase 3dB but because the amplifiers has to be driven in the same power levels as before, one must add another 3dB to the input of the power divider. Be aware that in the measurements a 1:4 power divider was used and therefore the power was increased 6dB.

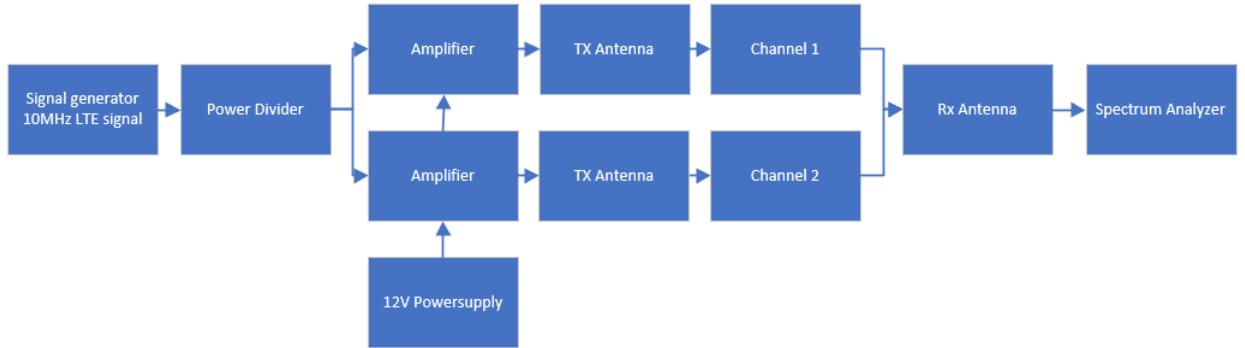


Figure 5.6: Block diagram of measurement using two antennas

In figure 5.7 a picture of a real measurement setup is shown. The antennas are spaced 1 meter apart from the input terminals and are pointing directly towards each other. The PA is mounted on a aluminium sheet with a tool grip to keep it at a constant temperature. The PA is supplied with 12.0VDC from the power supply and draws 40mA of current. The signal generator is connected to the input of the amplifier and the output of the amplifier is connected to the Tx antenna. The spectrum analyser is connected to Rx antenna.

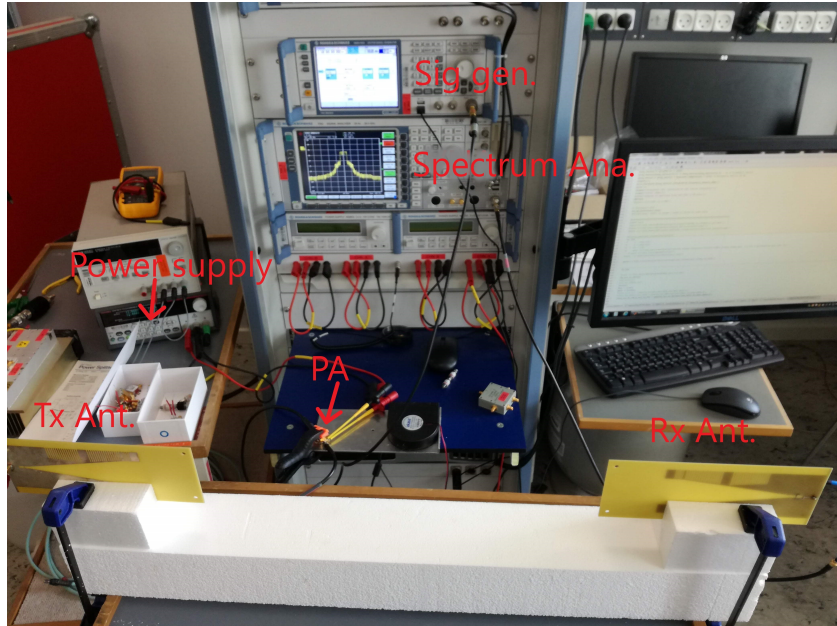


Figure 5.7: Measurement setup

5.2.1 Measurement of AM/AM distortion

Measurement has been done using the methods described in section 5.2. The results in figure 5.8 is a measurement of only the amplifier. It is seen that at an input of -2.5dB the amplifier starts to decrease its gain. This is expected due to the compression point. The mean gain of the amplifier is measured closely to 13.8dB as expected. It is further seen that the spreading of the signal is highest at low signal levels. When introducing one Tx antenna and one Rx antenna the free space loss must be accounted for. This is done by use of equation 5.1 which gives 20.5dB in loss. In the measurement 19.5dB was obtained, the difference is might caused by the antenna them self, since the used antenna gain is only simulated, and the antenna are spaced relatively close, or it can be reflections from the table that are causing the difference. Cable loss and connector loss has been measured and accounted for.

$$\text{Pathloss}(db) = 10 * \log_{10}(G_r G_t (\frac{4\pi d}{\lambda})^2) = 20.5dB \quad (5.1)$$

The measurement using one Tx antenna and one Rx antenna shows that the gain of the system now becomes close to 6dB, this is also expected since the gain of the system is:

$$G_{\text{system}}(dB) = G_{\text{amplifier}} + G_{\text{antenna}} - \text{Pathloss} = 13.85dB + 11.4dB - 19.5dB = 5.75dB \quad (5.2)$$

It can be seen from figure 5.9 that the antenna system makes the AM/AM distortion wider at the compression point, but smaller at lower power levels. In figure 5.10

to 5.15 the results from measurement setup three is shown. The results are made with two transmit antennas and therefore the system gain is increased by 3dB. The results shows small variations due to AM/AM distortion between, but a significant change in AM/AM at compression point in the pre-sentence of two antennas instead of one. Also AM/AM at lower power levels seems to decrease with two antennas compared to one.

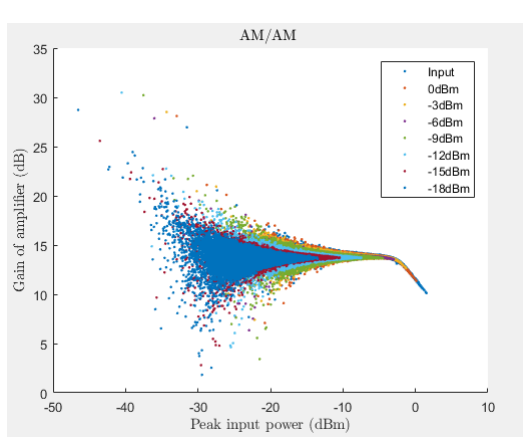


Figure 5.8: AM/AM distortion at amplifier

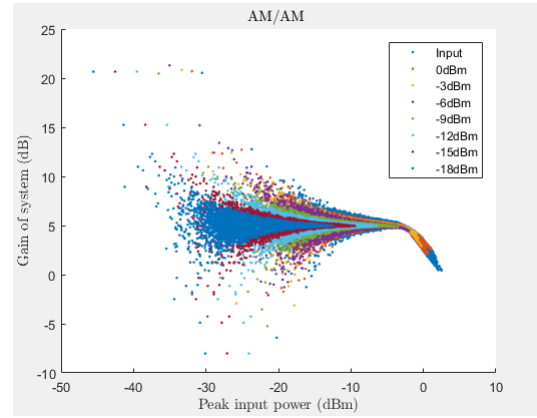


Figure 5.9: AM/AM distortion using one transmit antenna

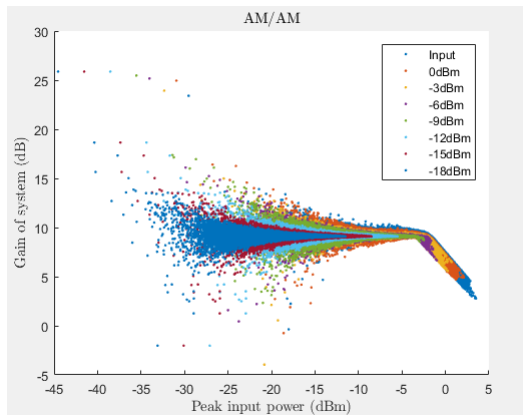


Figure 5.10: AM/AM distortion at 0.1λ

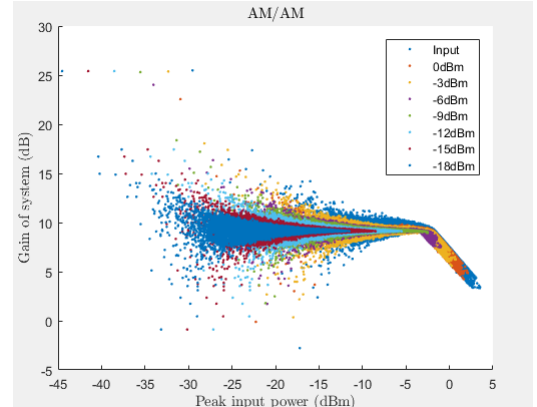


Figure 5.11: AM/AM distortion at 0.2λ

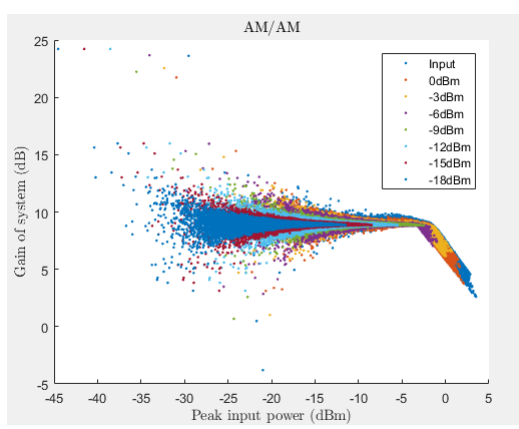


Figure 5.12: AM/AM distortion at 0.3λ

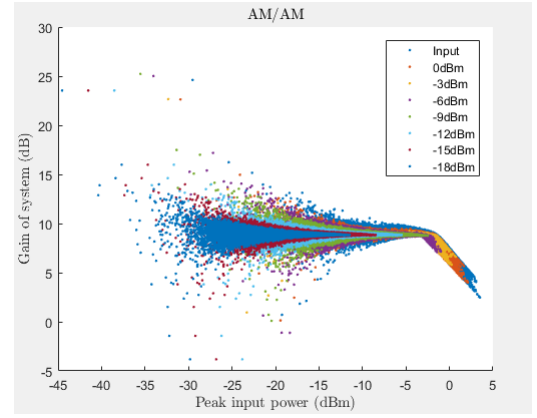


Figure 5.13: AM/AM distortion at 0.4λ

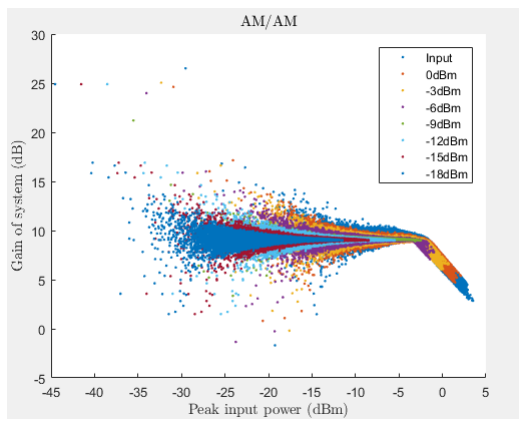


Figure 5.14: AM/AM distortion at 0.4λ

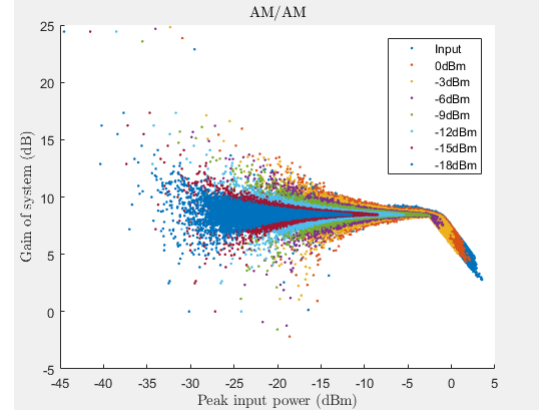
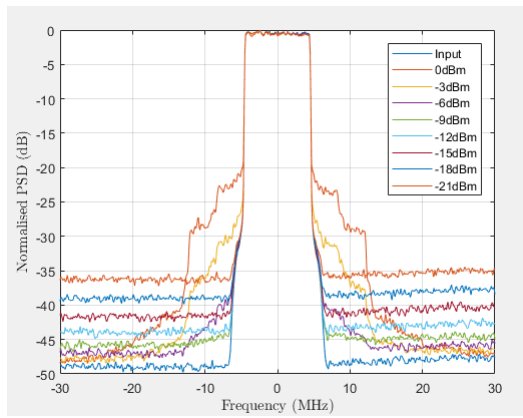
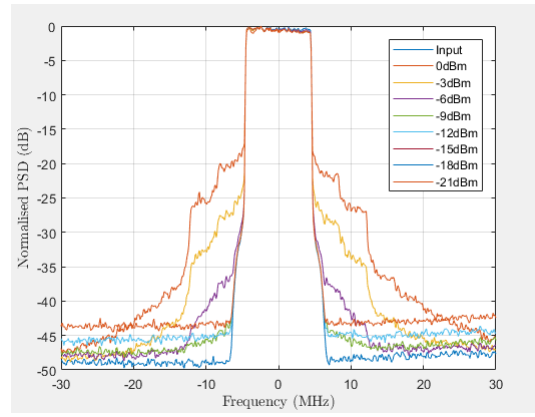
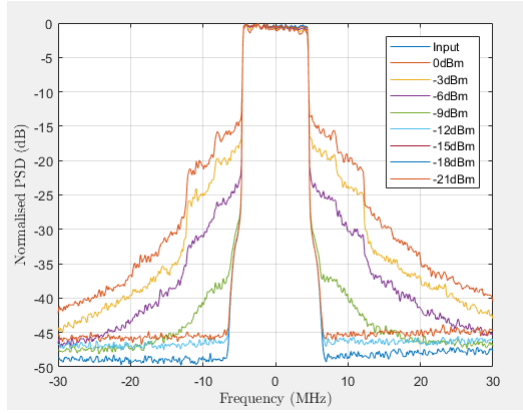
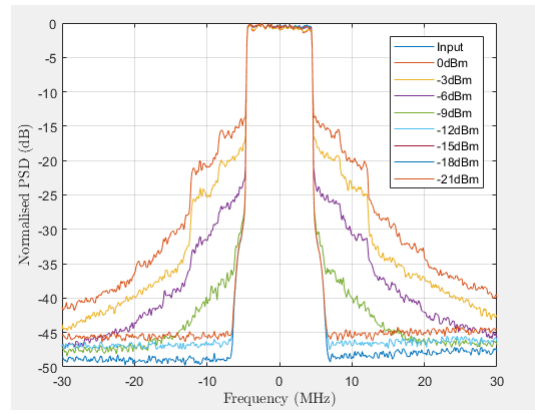
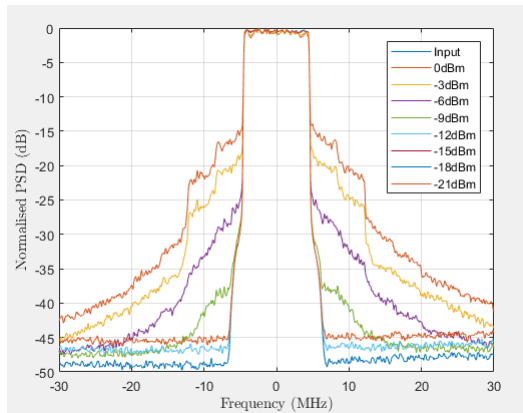
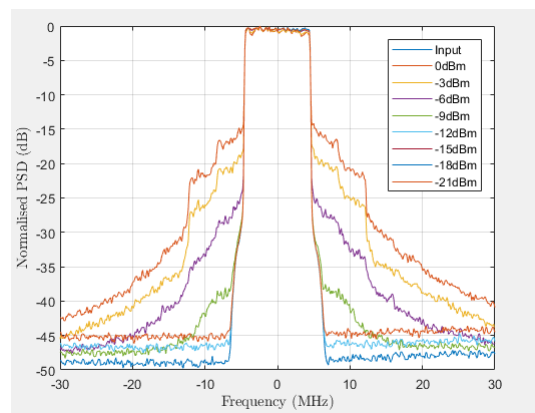
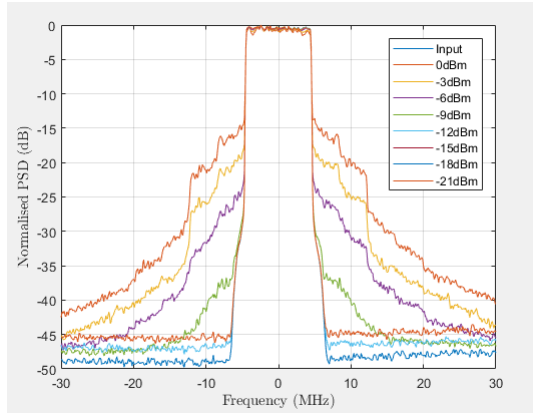
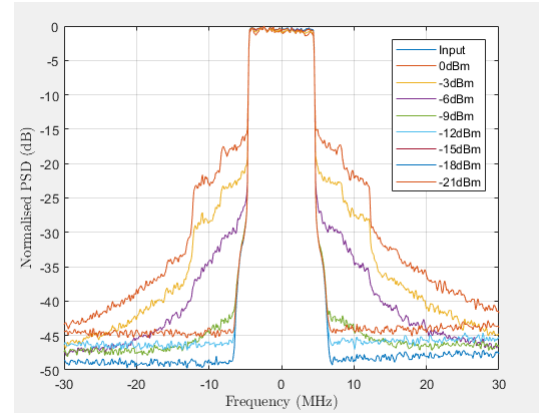


Figure 5.15: AM/AM distortion at 0.5λ

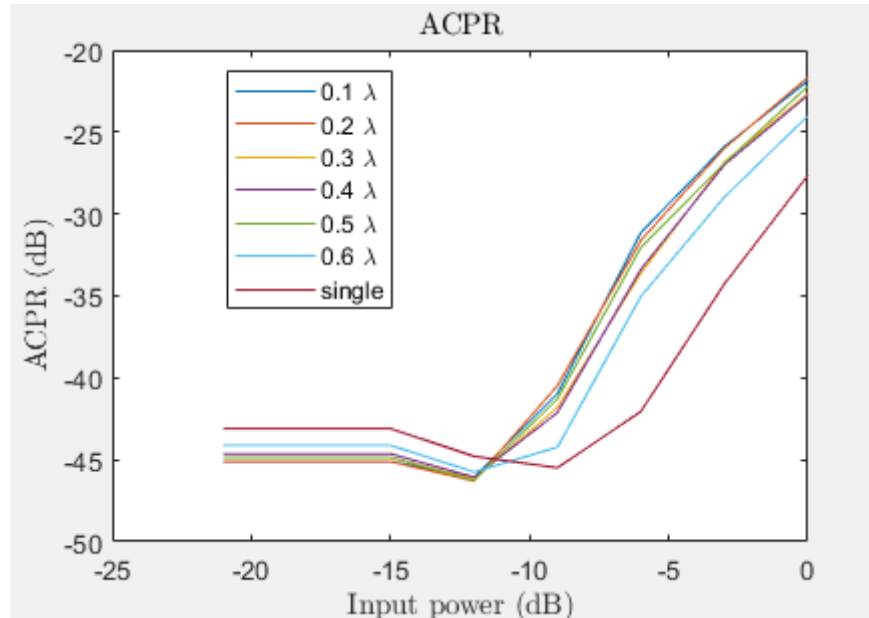
5.2.2 PSD

The Power Spectral Density (PSD) shown in figure 5.16 is measured directly at the amplifier. It shows that at a mean input-power at 0dBm the output of the amplifier is distorted, first at an input level at -9dBm the distortion becomes low. This is also expected since the input is mean power and therefore the peak of the signal would be closely to -3dBm (6dB backoff) which also is close to the compression point measured in section 5.2.1. Be aware that the noise floor increases due to the normalization of the signal. Also the reference-level at the spectrum analyser has an impact. When introducing the antenna system with one Tx antenna the distortion at -9dBm increases slightly. When introducing two antennas the distortion increases which is not a surprise due to the results from section 5.2.1.

**Figure 5.16:** PSD at amplifier**Figure 5.17:** PSD using one transmit antenna**Figure 5.18:** PSD at 0.1λ **Figure 5.19:** PSD at 0.2λ **Figure 5.20:** PSD at 0.3λ **Figure 5.21:** PSD at 0.4λ

**Figure 5.22:** PSD at 0.5λ **Figure 5.23:** PSD at 0.6λ

5.2.3 ACPR

**Figure 5.24:** ACPR

Chapter 6

Conclusion

The purpose of this project was to development an antenna to receive ADS-B signals from aircraft's on a CubeSat. A link budget was made and it showed that there was a need for a radiation-pattern that could compensate for the increased length in the reception due to the angle of the earth. Another important requirement for the antenna was that it should be circular-polarized since the received signal was linear polarized but the angle of reception was not known. A reflector antenna, a quadrifilar helical antenna and a hemispherical antenna was investigated. None of these antenna could overcome those requirements in their basic forms and modifications to these was investigated. The reflector antenna had a high gain in one single direction and a large size compared to the wavelength which made it difficult to use on a CubeSat. The quadrifilar helical antenna showed that is was difficult to change in its radiation-pattern due to the common design and still keep it circular polarized. The hemispherical helical antenna was modified to have four arms and a stretched structure which showed good performance, but this design had no gain in the center. This could be improved by changing the feeding point, but this introduced a non-symmetry which made the antenna to become non circular polarized.

Bibliography

- Ali Cheaito, e. a. (2016). Evm derivation of multicarrier signals to determine the operating point of the power amplifier considering clipping and predistortion. ResearchGate.
- Balanis, C. A. (2005). *Antenna Theory Analysis And Design*. Wiley, 3. ed. edition.
- Clark, J. R. (2003). Multifilar hemispherical helical antennas. Virginia Polytechnic Institute and State University.
- Francis, e. a. (2011). The flying laboratory for the observation of ads-b signals. <https://www.hindawi.com/journals/ijno/2011/973656/>.
- ITU-R (2017). Reception of automatic dependent surveillance broadcast via satellite and compatibility studies with incumbent systems in the frequency band 1087.7-1092.3 mhz. https://www.itu.int/dms_pub/itu-r/opb/rep/R-REP-M.2413-2017-PDF-E.pdf.
- Iyer, V. (2010). Broadband impedance matching of antenna radiators. <https://web.wpi.edu/Pubs/ETD/Available/etd-092910-012955/unrestricted/viyer.pdf>.
- Katharina Hausmair, e. a. (2017). Digital predistortion for multi-antenna transmitters affected by antenna crosstalk. http://www.ieee.org/publications_standards/publications/rights/index.html.
- Molisch, A. F. (2011). Wireless communications.
- National-Instruments (2019). Optimizing ip3 and acpr measurements. www.ni.com/rf-academy.
- Shkelzen Cakaj, e. a. (2014). The coverage analysis for low earth orbiting satellites at low elevation. International Journal of Advanced Computer Science and Applications, Vol. 5, No. 6, 2014.
- Sun, J. (2015). The 1090mhz riddle. <https://mode-s.org/decode/>.
- Taijun Liu, e. (2007). Memory effect pre-compensation for wideband rf power amplifiers using fir-based weak nonlinear filters. <https://ieeexplore.ieee.org>.

- William A. Imbriale, e. a. (2012). *Space Antenna Handbook*. Wiley, 1. ed. edition.
- Xiaoqiang Yang, e. a. (2014). A broadband printed quadrifilar helical antenna with a novel compact broadband feeding network. Progress In Electromagnetics Research C, Vol. 51, 103–109, 2014.
- Xuan Wang, e. a. (2011). Correlation coefficient expression by s-parameters for two omni-directional mimo antennas. <https://ieeexplore.ieee.org/stamp/stamp.jsp?arnumber=5996702>.
- Xudong Bai, e. a. (2014). Compact design of triple-band circularly polarized quadrifilar helix antennas. IEEE antennas and wireless propagation letters, VOL. 13 2014.
- Yan Guo, e. a. (2015). Power adaptive digital predistortion for wideband rf power amplifiers with dynamic power transmission. IEEE TRANSACTIONS ON MICROWAVE THEORY AND TECHNIQUES, VOL. 63, NO. 11, NOVEMBER 2015.
- Zahidul Islam Shahin, e. a. (2017). Efficient dpd coefficient extraction for compensating antenna crosstalk and mismatch effects in advanced antenna system. Department of Electrical and Information Technology LTH, Lund University SE-221 00 Lund, Sweden.

Appendix A

Appendix A name

Here is the first appendix